J. Fluid Mech. (1984), *vol.* 140, *pp.* 189–222
Printed in Great Britain

Calculation of turbulence-driven secondary motion in non-circular ducts

By A. O. DEMUREN AND W. RODI
Institut für Hydromechanik, University of Karlsruhe, Karlsruhe, F.R. Germany

(Received 30 November 1982 and in revised form 13 November 1983)

Experiments on and calculation methods for flow in straight non-circular ducts involving turbulence-driven secondary motion are reviewed. The origin of the secondary motion and the shortcomings of existing calculation methods are discussed. A more refined model is introduced, in which algebraic expressions are derived for the Reynolds stresses in the momentum equations for the secondary motion by simplifying the modelled Reynolds-stress equations of Launder, Reece & Rodi (1975), while a simple eddy-viscosity model is used for the shear stresses in the axial momentum equation. The kinetic energy k and the dissipation rate ϵ of the turbulent motion which appear in the algebraic and the eddy-viscosity expressions are determined from transport equations. The resulting set of equations is solved with a forward-marching numerical procedure for three-dimensional shear layers. The model, as well as a version proposed by Naot & Rodi (1982), is tested by application to developing flow in a square duct and to developed flow in a partially roughened rectangular duct investigated experimentally by Hinze (1973). In both cases, the main features of the mean-flow and the turbulence quantities are simulated realistically by both models, but the present model underpredicts the secondary velocity while the Naot–Rodi model tends to overpredict it.

1. Introduction

Turbulent flows in ducts or passages of non-circular cross-section are often encountered in engineering practice. Examples are flows in heat exchangers, ventilation and air-conditioning systems, nuclear reactors, turbomachinery, open channels, canals and rivers. The flow in such ducts is accompanied by secondary motions in the plane perpendicular to the streamwise direction, and this secondary motion can be caused by two different mechanisms. In curved ducts, where centrifugal forces act at right angles to the main flow direction, this motion is pressure-induced and is said to be of Prandtl's first kind. This kind also exists in curved circular ducts and for laminar flow, and the secondary velocities can be quite large, say of the order of 20–30 % of the bulk streamwise velocity. Secondary motion of Prandtl's second kind is encountered in non-circular straight ducts, and, since, in contrast with laminar flow, this secondary motion is present also under fully developed conditions, it is caused by turbulence. The present paper is concerned with turbulence-driven secondary motion, which has been observed in non-circular ducts and open channels. Although the secondary velocity is only of the order of 2–3 % of the streamwise bulk velocity, this motion can have important consequences. By transporting high-momentum fluid towards the corners, it causes a bulging of the velocity contours towards the corners. In open-channel flows, this secondary motion moves fluid with relatively low streamwise momentum towards the centre portion of the channel and causes the

observed depression of the velocity maximum below the surface. Furthermore, the secondary motion produces an increase of the wall shear stress towards corners, an effect which is of great importance for sediment-transport and erosion problems. Similarly, the heat transfer at duct walls is influenced significantly by the secondary motions, and these can also significantly increase the lateral spreading of any tracer discharged into a channel. For these reasons it is important to understand and be able to accurately predict secondary-flow phenomena in developing flow situations and in the asymptotic developed state. The present paper introduces a general three-dimensional model for simulating these flow situations.

2. Previous work and present contribution

2.1. *Experiments*

A considerable number of experimental investigations have been carried out on turbulent flow in straight non-circular ducts. These investigations can be classified broadly into two categories: (i) those concerned with the influence of duct geometry on friction laws and on laws for the longitudinal velocity distribution; and (ii) those concerned with the secondary motion, its origin and its effect on various global and local flow properties. In this paper, the findings of the second category are of prime interest and will be discussed in greater detail below. The earlier measurements of the first category indicated that the friction factor for fully developed turbulent duct flows could be closely correlated by the Blasius formula for circular pipes when the Reynolds number was based on the hydraulic diameter. More extensive later studies have shown, however, that there is no unique, geometry-independent relationship between the friction factor and the Reynolds number based on the hydraulic diameter. Hence consideration of the details of the duct geometry appears to be important. The experimental investigations of the first category have also shown that, except in immediate corner regions ($x_2^+ < 30$ and $x_3^+ < 30$), the usual inner logarithmic law of the wall is valid, with scatter in the involved constants only slightly larger than for different circular pipe-flow experiments. In contrast to such flows, however, no universal defect laws were found for the outer region, except in elliptic ducts.

Experiments on detailed flow development, including the secondary motion, will now be discussed. Nikuradse (1930) was perhaps the first one to observe the secondary motion in non-circular ducts by flow-visualization studies. These studies were conducted in order to explain the cause of the bulging of the axial-velocity contours towards the corner which he had observed in his earlier experiments.

However, it took another 30 years before Hoagland (1960) reported the first actual measurements of the secondary motion. Subsequently, such measurements have been reported by Brundett & Baines (1964), Gessner (1964, also presented in Gessner & Jones 1965), Launder & Ying (1972), Melling & Whitelaw (1976), Po (1975), Lund (1977) and Gessner & Emery (1980) in square ducts, Gessner (1964) and Tracy (1965) in rectangular ducts, and by Aly, Trupp & Gerrard (1978) in a triangular duct. The findings of these measurements will now be summarized and evaluated.

Approach to developed flow

Details of some experimental results for developing duct flow will be presented below together with the calculations. Here the question is posed whether the individual experiments were carried out to sufficiently large downstream distances for fully developed flow to prevail. Unfortunately this question cannot be answered with certainty in most cases. Melling & Whitelaw (1976) presented measurements of

the developing flow in a square duct at various cross-sections up to $36.8D_h$ (D_h = hydraulic diameter), at which station the flow was far from fully developed. Various aspects of developing square-duct flow have been investigated in complementary studies by Po (1975), Lund (1977) and Gessner (see Gessner & Emery 1980), all using the same experimental facility. These measurements were conducted at a number of cross-sections down to a streamwise location of $84D_h$. The streamwise velocity at the centreline, relative to the bulk velocity, increased monotonically down to about $40D_h$, where it reached a maximum. Further downstream, it decreased until $70D_h$, beyond which it was practically constant at 70 % below the peak value. Gessner's measured secondary velocity increased between $40D_h$ and $84D_h$ by about 10 % along the wall bisector and by 50 % along the corner bisector. Po's measurements of the Reynolds stresses showed a decrease of 10–20 % between these two cross-sections. Since no measurements are reported between $40D_h$ and $84D_h$ and beyond $84D_h$, no definite conclusions can be drawn as to whether the flow was fully developed at $84D_h$. In a recent survey on the development of turbulent pipe flow, Klein (1981) found that the length required for full flow development may exceed 140 pipe diameters. However, for certain inlet conditions it was found to be as low as 70 diameters. The development length for flow in non-circular ducts must be expected to be of the same order of magnitude if not larger because the secondary motion may take longer to reach a developed state. It is interesting to note, however, that the centreline velocity in many of the data reviewed by Klein attained a peak value at about 40 diameters, which compares well with the peak at $40D_h$ measured by Gessner in the square duct.

Brundett & Baines' (1964) measurements at $260D_h$ must be assumed to be for developed flow, while in the duct of Launder & Ying (1972) the flow was probably not fully developed at the measurement cross-section $x_1/D_h = 69$, as will be discussed further below.

Results for approximately developed flow

Velocity contours of various experimenters measured at the furthest downstream station are compared in figure 1. These contours show the typical bulging towards the corner which is caused by the secondary motion. The contours of Launder & Ying show considerably less bulging in the centre portion of the duct than do the other measurements. This is consistent with the smaller secondary motion measured by these authors (see figure 3), so that the buildup of the secondary motion was probably not completed by $69D_h$ and the flow there was not fully developed. Launder (private communication 1982) agrees with this conclusion. Some of the differences between the remaining experimental results are due to differences in the Reynolds number. Figure 2 shows that the ratio of maximum (centreline) velocity to bulk velocity U_b decreases somewhat with increasing Reynolds number, and this may explain partly the differences in the contours of Brundett & Baines on the one hand and Po and Lund on the other. However, the latter two authors conducted their experiments in the same apparatus; the differences between their results are therefore an indication of the experimental uncertainty. It should also be mentioned that the contours 1.10, and to a lesser extent 1.05, in figure 1, magnify small differences in the velocity distribution because of the small gradients of the velocity profiles in the centre portion.

While there was no clear variation of the ratio of the centreline velocity to bulk velocity with Reynolds number beyond $Re = 120000$, the friction velocity relative to the bulk velocity, whose Reynolds-number dependence is also plotted in figure 2, was found to decrease continuously with increasing Re in the whole range investigated.

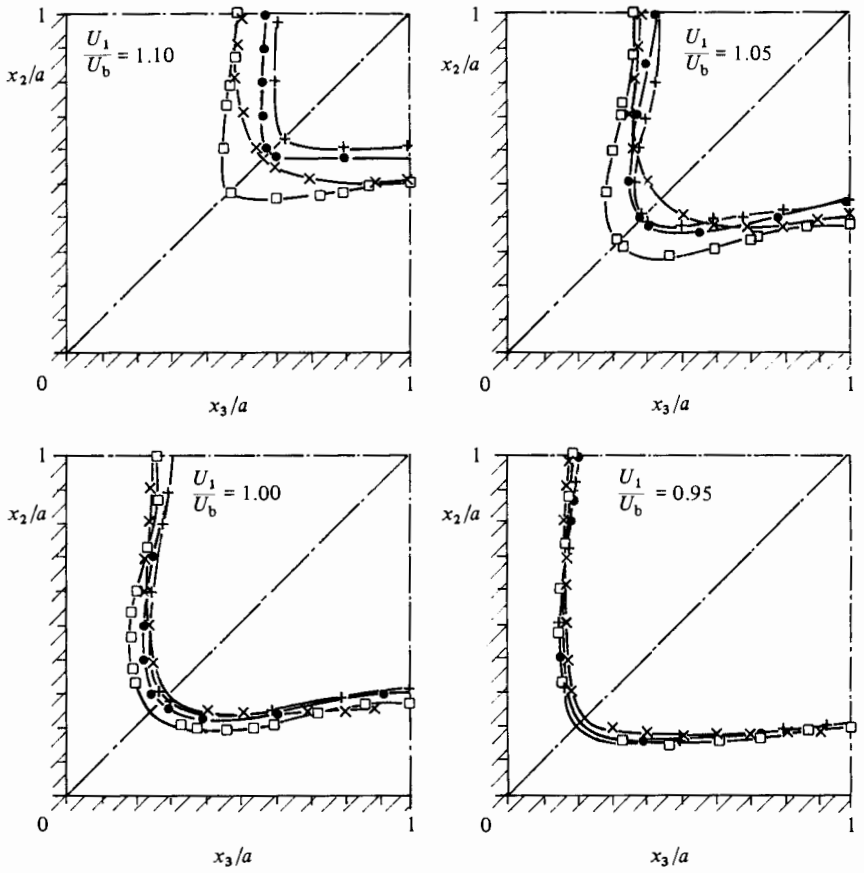

FIGURE 1. Measured contours of primary velocity: -+-+-, Po (1975); -●-●-, Lund (1977); -×-×-, Launder & Ying (1972); -□-□-, Brundett & Baines (1964).

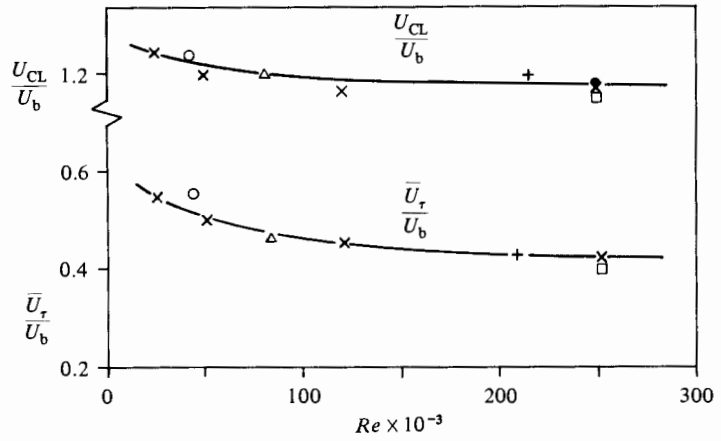

FIGURE 2. Influence of Reynolds number on friction and axial centreline velocities. Data: ×, Lund (1977); △, Brundett & Baines (1964); □, Po (1975); +, Launder & Ying (1972); ●, Gessner (in Gessner & Emery 1980); ——, present predictions.

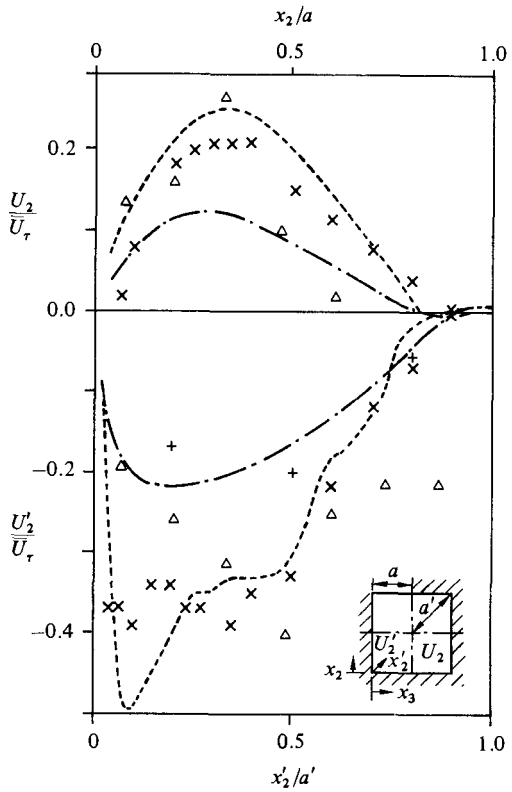

FIGURE 3. Secondary velocities along wall and corner bisectors. Data: △, Brundett & Baines (1964); +, Launder & Ying (1972); ×, Gessner (in Gessner & Emery 1980). Predictions: —·—, present model; ---, Naot & Rodi's (1982) model.

Launder & Ying (1972) have argued that the effect of Reynolds number on the secondary motion can be reduced if not eliminated by normalizing the secondary velocities with the friction velocity rather than with the bulk velocity. Figure 3 shows secondary velocities along the wall bisector and corner bisector measured at the most-downstream station in various experiments.

Normalizing the secondary velocities with the friction velocity can be seen to bring the level of the relative secondary velocity measured by various experimenters to a reasonable accord. The level of Launder & Ying's secondary motion is markedly lower than that of other experiments, indicating that the secondary motion was still building up. The considerable scatter of the data shown in figure 3 also points to the fact that the relatively small secondary velocities are very difficult to measure accurately. The scatter gives a realistic indication of the uncertainties involved in the secondary velocity data. These uncertainties appear to be of the same order as differences that may arise due to different Reynolds numbers.

Origin of the secondary motion

The measurements reviewed above have shown the magnitudes and effects of the secondary motion, but they give no indication as to its origin. Prandtl (1926) was the first to suggest that the secondary motion in non-circular straight ducts was caused by the turbulence field, but it was not until Einstein & Li (1958) that a rigorous analysis was carried out to show that it is the gradients of Reynolds stresses that

give rise to the secondary motion. In order to examine experimentally the origin of the secondary motion, Brundett & Baines (1964) measured all three velocity and all six Reynolds-stress components in a fully developed square-duct flow and used these measurements to examine the magnitude of the terms in the streamwise vorticity equation. For a steady incompressible constant-property flow, the equation for the streamwise vorticity Ω_1 has the following exact form (in the coordinate system given in figure 4):

$$\underbrace{U_1\frac{\partial\Omega_1}{\partial x_1}+U_2\frac{\partial\Omega_1}{\partial x_2}+U_3\frac{\partial\Omega_1}{\partial x_3}}_{A_1}-\underbrace{\Omega_1\frac{\partial U_1}{\partial x_1}-\Omega_2\frac{\partial U_1}{\partial x_2}-\Omega_3\frac{\partial U_1}{\partial x_3}}_{A_2}$$

$$=\underbrace{\frac{\partial}{\partial x_1}\left(\frac{\partial\overline{u_1u_2}}{\partial x_3}-\frac{\partial\overline{u_1u_3}}{\partial x_2}\right)}_{A_3}+\underbrace{\frac{\partial^2}{\partial x_2\,\partial x_3}(\overline{u_3^2}-\overline{u_2^2})}_{A_4}-\underbrace{\left(\frac{\partial^2}{\partial x_3^2}-\frac{\partial^2}{\partial x_2^2}\right)\overline{u_2u_3}}_{A_5}$$

$$+\underbrace{\nu\left(\frac{\partial^2\Omega_1}{\partial x_1^2}+\frac{\partial^2\Omega_1}{\partial x_2^2}+\frac{\partial^2\Omega_1}{\partial x_3^2}\right)}_{A_6}, \tag{1}$$

where the components of the vorticity vector are

$$\Omega_1=\frac{\partial U_2}{\partial x_3}-\frac{\partial U_3}{\partial x_2},\quad \Omega_2=\frac{\partial U_1}{\partial x_3}-\frac{\partial U_3}{\partial x_1},\quad \Omega_3=\frac{\partial U_2}{\partial x_1}-\frac{\partial U_1}{\partial x_2}. \tag{2}$$

The terms A_1 represent the convection of the streamwise vorticity by the mean motion, and the terms A_2 the vortex stretching and tilting by the mean-velocity gradients; the latter form the source of secondary motion of Prandtl's first kind. The terms A_3, A_4 and A_5 express the influence of the turbulent stresses on the production or destruction of streamwise vorticity, and A_6 the damping by viscosity. Brundett & Baines considered only fully developed flow, in which case all gradients with respect to x_1 (streamwise direction) are zero, and (1) reduces to

$$\underbrace{U_2\frac{\partial\Omega_1}{\partial x_2}+U_3\frac{\partial\Omega_1}{\partial x_3}}_{A_1}=\underbrace{\frac{\partial^2}{\partial x_2\,\partial x_3}(\overline{u_3^2}-\overline{u_2^2})}_{A_4}-\underbrace{\left(\frac{\partial^2}{\partial x_3^2}-\frac{\partial^2}{\partial x_2^2}\right)\overline{u_2u_3}}_{A_5}+\underbrace{\nu\left(\frac{\partial^2\Omega_1}{\partial x_2^2}+\frac{\partial^2\Omega_1}{\partial x_3^2}\right)}_{A_6}. \tag{3}$$

They then evaluated each term in (3) from their measurements as well as from those of Hoagland (1960), using simple finite-difference relations to determine the gradients from the 8×8 measurement grid. This evaluation yielded that, of the two turbulent-stress terms, only A_4 was significant and was balanced by the convection and viscous-damping terms A_1 and A_6. Brundett & Baines then concluded that streamwise vorticity was produced by A_4 and then convected by A_1 to regions where the vorticity was destroyed by the viscous-damping term A_6. Perkins (1970) pointed out that the hot-wire procedure of Brundett & Baines involved rotating a single-wire sensor to eight different orientations at each point in the flow, so that the turbulent stress terms $\overline{u_2u_3}$ and $\overline{u_3^2}-\overline{u_2^2}$ were each obtained from 4 measured r.m.s. voltages, and that an error of $\pm1\,\%$ in each r.m.s. voltage could lead to an error of $\pm100\,\%$ in the shear stress $\overline{u_2u_3}$. Further, the differentiation from 8×8 measurement points introduced additional inaccuracies so that the results of Brundett & Baines are not very reliable.

Gessner & Jones (1965) used an X-array hot-wire probe which enabled the Reynolds

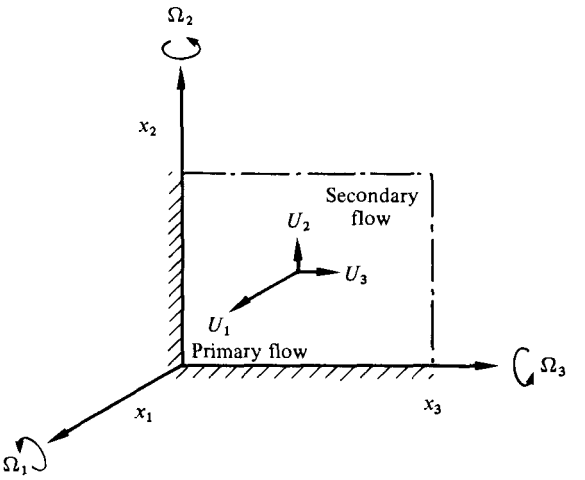

FIGURE 4. Coordinate system for rectangular-channel flow.

stresses to be measured more accurately. They derived a momentum equation for the velocity component along a secondary-flow streamline and measured the terms in this equation at points located on this streamline as well as the normal gradients by moving the hot wire normally to the streamline at each point. This way, the individual terms in the momentum equation could be measured quite accurately, and the evaluation of the results showed that the convection and viscous terms were both two orders of magnitude smaller than the turbulent-stress terms (the viscous term was significant only near the corner, where its magnitude reached about half that of the convective term). The turbulent normal and shear-stress terms, which lead to the terms A_4 and A_5 in the vorticity equation (3) when the latter is derived from the momentum equations, emerged to be of the same order of magnitude, and their sum was seen to be balanced by the pressure-gradient term. The last term could not be measured but was determined from the difference of the other terms. The pressure term is, of course, not a source of vorticity, because it disappears when the vorticity equation (3) is derived from the momentum equations. The findings of Gessner & Jones contradict those of Brundett & Baines in so far as the former found the viscous terms to be negligible and the secondary motion to be produced by the difference between turbulent stress terms. The fact that, in contrast with Brundett & Baines' experiments, Gessner & Jones' measurements were not in fully developed flow does not explain these severe differences. Rather they are due to the inaccurate method of Brundett & Baines in measuring and differentiating the turbulent stresses.

Perkins (1970) investigated experimentally the mechanism for generating streamwise vorticity in turbulent corner flow developing at approximately constant pressure. This flow situation is virtually the same as that in corners of developing duct flow and he found that the individual Reynolds stresses indeed behaved very much the same as in the square-duct flow studied by Gessner & Jones. Considering the streamwise vorticity balance in (1), he found that all the terms involving streamwise gradients were negligible except $U_1 \partial\Omega_1/\partial x_1$, which varied erratically. The turbulent normal and shear-stress terms came out to be of the same order of magnitude and of opposite sign, confirming Gessner & Jones' findings. Perkins argued that two different mechanisms contribute to the generation of the secondary shear stress $\overline{u_2 u_3}$. The first mechanism is associated with the gradients of the secondary

velocities, and its contributions to $\overline{u_2 u_3}$ can be represented in terms of an isotropic eddy viscosity. The second mechanism is associated with the distortion of the primary stress field in the corner and is therefore associated with the primary velocity gradients. Although the individual contributions to the generation of $\overline{u_2 u_3}$ could not be determined from the experiment, Perkins considered them to be of equal magnitude. It will be shown below that it is indeed important to represent both processes in a mathematical model.

Contrary to all previous beliefs, Gessner (1973) claimed that the anisotropy of the turbulent normal stresses do not play a major role in the generation of the secondary motion. Since all the terms in the streamwise vorticity equation (1) are at least an order of magnitude smaller than the terms in the equations for the other vorticity components (involving gradients of the primary velocity which are much larger than those of the secondary velocities), he argued that these equations should be examined instead of the Ω_1 equation in order to explain the origin of the secondary motion. He evaluated the terms in a transformed equation for the vorticity along the corner bisector, using his experimental results obtained specifically for this purpose. Based on these data, he argued that the conversion of mean-flow vorticity to turbulent vorticity by the transverse gradients of the primary shear stresses occurring in the corner region could only be balanced by convection of mean-flow vorticity by secondary motions into this region. Thus he inferred that the secondary motion is due to transverse gradients of the primary shear stresses in the corner region. He reached similar conclusions from energy considerations. These findings are certainly not inconsistent with those of others, but they do not *explain* the generation of the secondary motion. This is directly associated with the streamwise vorticity Ω_1, and only equation (1) or (3) for this quantity can show how this is generated; and, since the turbulent normal and shear stresses in the cross-sectional plane appear prominently in this equation, they do play an important role in the vorticity generation.

The experimental findings on the generation of secondary motion in non-circular straight ducts may be summarized as follows. In the Ω_1 equation (1) or (3), the turbulent-stress terms A_4 and A_5 are the dominant ones, being of opposite sign and much larger than the convection terms A_1. The viscous terms A_6 are negligible except very close to the corner. Hence the difference between A_4 and A_5 is of the same order of magnitude as the convection terms, and it is this difference between these relatively large terms that drives the secondary motion. As a consequence, both terms A_4 and A_5 must be modelled accurately in a mathematical simulation in order to describe realistically the secondary flow.

2.2. *Previous calculations*

The first calculation of secondary flow in straight non-circular ducts was carried out by Launder & Ying (1973). These authors recognized that a model using an isotropic eddy viscosity for calculating the turbulent stresses in the streamwise vorticity equation (1) does not produce any secondary motion at all and that more refined modelling of these stresses is required. Accordingly they derived a model for the stresses $\overline{u_3^2} - \overline{u_2^2}$ and $\overline{u_2 u_3}$ by simplifying the transport equations for these stresses given in model form by Hanjalić & Launder (1972). From these differential equations, algebraic expressions for the above stresses were obtained by neglecting the convection and diffusion terms (assumption of local equilibrium) and by further neglecting all secondary velocity gradients. The primary shear stresses $\overline{u_1 u_2}$ and $\overline{u_1 u_3}$ were calculated from a standard eddy-viscosity model. The turbulent kinetic energy k appearing

in the stress relations was obtained by solving a transport equation for k, and the distribution of the length-scale L was determined from the algebraic geometrical formula of Buleev (1963). This algebraic stress model denoted LY has been used (sometimes with slight modifications) by a number of other authors in calculating a fairly wide range of straight duct flows. Tatchell (1975) replaced the algebraic length-scale formula by a transport equation for the dissipation rate $\epsilon (L \propto k^{\frac{3}{2}}/\epsilon)$. This model represents a generalization of the LY-model and has been favoured especially in calculations of the flow in channels with complex geometrical cross-sections. Ramachandra (1979) and Gosman & Rapley (1980) used such a method to calculate, with a fair degree of success, fully developed flow in square ducts, triangular ducts and ducts with rod-bundle geometries. Gessner & Emery (1980) have also employed modified versions of the LY-model in calculating developing and fully developed rectangular channel flows.

In all the applications of the LY-model and its modifications, roughly the correct level of secondary motion has been obtained. At first, this is somewhat surprising in view of the finding of Kacker (1973) that the LY-model predicts the separation between the two normal stresses $(\overline{u_3^2}-\overline{u_2^2})/U_\tau^2$ which drives the secondary motion, to be too small by a factor of roughly 10. The algebraic stress relations of LY read

$$\overline{u_3^2}-\overline{u_2^2} = c'\frac{k}{\epsilon}\left(\overline{u_1 u_3}\frac{\partial U_1}{\partial x_3}-\overline{u_1 u_2}\frac{\partial U_1}{\partial x_2}\right), \quad \overline{u_2 u_3} = c'\frac{k}{\epsilon}\left(\overline{u_1 u_2}\frac{\partial U_1}{\partial x_3}+\overline{u_1 u_3}\frac{\partial U_1}{\partial x_2}\right). \tag{4}$$

In the parent stress-equation model, Hanjalić & Launder (1972) recommended a value for the empirical coefficient of $c' = 0.067$. Apparently this coefficient produced too large a secondary motion, and hence LY adopted the smaller value of $c' = 0.0185$ in their secondary-flow calculations. Even the higher value of $c' = 0.067$ underpredicts the separation between the normal stresses $\overline{u_3^2}$ and $\overline{u_2^2}$ by a factor of 2–3. This is due to the fact that Hanjalic & Launder took no account in their model of the effects of wall proximity on the individual stresses which damp the fluctuations normal to the wall and enhance the ones parallel to the wall. The fact that the correct level of secondary motion is predicted by the LY-model even though the driving term $\overline{u_3^2}-\overline{u_2^2}$ is too small by a factor of 10 is due to the neglect of secondary velocity gradients in the algebraic stress model. As was discussed already, Perkins (1970) pointed out that the secondary velocity gradients contribute significantly to the generation of the secondary shear stress $\overline{u_2 u_3}$. When this is neglected, the sink term A_5 in the vorticity equation (1) is reduced significantly, and, since the secondary motion is governed by a subtle balance between A_4 and A_5, the driving term A_4 must also be reduced to unrealistically small values. One may therefore conclude that the LY-model produces the correct secondary motion for the wrong reason. As will be shown in §4.7, the contribution of the secondary velocity gradients to the shear stress $\overline{u_2 u_3}$, neglected in the LY-model, is in reality larger than the contribution by the primary velocity gradients over much of the flow domain in a fully developed square-duct flow.

Launder, Reece & Rodi (1975) proposed a Reynolds-stress-equation model which accounts for near-wall effects on the turbulent fluctuations by a special wall-proximity correction to the pressure–strain model. This model yields a separation between the normal stresses $\overline{u_3^2}$ and $\overline{u_2^2}$ in agreement with experiments. Reece (1976) applied this Reynolds-stress-equation model to calculate developing flow in square ducts. He did not make the local equilibrium assumption but solved the differential transport equations for all six Reynolds stresses. The use of the Launder *et al.* pressure–strain model means that the coefficient c' in (4) is effectively more than 10 times as large as in the LY-model. Reece did not specifically mention whether he retained the

secondary velocity gradients in his model, but it seems likely that some account of these gradients was taken because otherwise a far too large secondary motion would have resulted. It may well have been that the secondary velocity gradients were accounted for approximately by an eddy-viscosity expression built into the computer program used by Reece similar to the procedure adopted by Naot & Rodi (1982) described below. Reece compared the calculated distributions of the three velocity components and five Reynolds stresses in developing square-duct flow with the measurements of Melling & Whitelaw (1976) and obtained good agreement.

Naot, Shavit & Wolfstein (1974) developed a Reynolds-stress-equation model similar to that of Launder *et al.* The main differences can be found in the empirical constants employed and in the fact that Naot *et al.* prescribed the lengthscale from geometrical considerations while Launder *et al.* calculated it by solving an equation for the dissipation rate ϵ. Naot *et al.* applied their model to fully developed square-duct flow. They did not neglect the secondary velocity gradients, but owing to the strong coupling of the differential equations of the mean flow and the Reynolds stresses they could not obtain a stable solution for Reynolds numbers higher than 2×10^5. Their calculated velocities and Reynolds stresses compared satisfactorily with the measurements of Brundett & Baines (1964, at $Re = 8.3 \times 10^4$) and of Gessner & Jones (1965, at $Re = 1.5 \times 10^5$). Since reservations have been expressed above about these data, this comparison is not entirely conclusive.

In a study preliminary to the present one, Naot & Rodi (1982), from here on referred to as NR, simplified the Reynolds-stress-equation model of Launder *et al.* to an algebraic-stress model and applied it to calculate the secondary motion in developed duct and open-channel flows. Similarly to LY, NR neglected the convection and diffusion terms in the Reynolds-stress equation (assumption of local equilibrium) and calculated the primary stresses with the standard eddy-viscosity model. However, the terms involving secondary velocity gradients in the modelled transport equation for $\overline{u_2^2}, \overline{u_3^2}$ and $\overline{u_2 u_3}$ were not neglected but approximated by products of an isotropic eddy viscosity and the corresponding secondary velocity gradients (the actual expressions will be presented below). NR found that, when these terms were neglected, the secondary motion grew without bounds and no stable solution could be obtained. Arnal & Cousteix (1981) experienced the same problems with a very similar model when the empirical constants suggested by Launder *et al.* were used. Rather than including the secondary-velocity-gradient terms, however, they brought about a realistic simulation of the secondary motion by changing one of the empirical constants, effectively reducing drastically the empirical constant c' in (4). As in the case of the LY-model, the correct secondary motion was thereby achieved by tuning the constants and not by a realistic simulation of the physical processes.

2.3. *Present contribution*

The importance of the secondary-velocity gradients in the Reynolds-stress equations and also in the simplified algebraic stress relations, particularly for $\overline{u_2 u_3}$, has been highlighted in the previous section. These gradients have been neglected in almost all previous calculations of the secondary motion in non-circular straight ducts, and this has been compensated for by tuning the empirical model constants in such a way that the actual driving term $\overline{u_3^2} - \overline{u_2^2}$ was much too small. Naot & Rodi accounted for these gradients in their model in an approximate way, which is, however, not entirely consistent with the treatment of the primary-velocity-gradient terms. One of the main objectives of this study is to extend the NR-model by treating the secondary-velocity-gradient terms exactly in the same way as the primary-gradient ones and

to examine quantitatively the influence of the secondary velocity gradients in the model. As in the NR-model, algebraic expressions are derived from the Reynolds-stress equations of Launder *et al.* by invoking the local equilibrium assumption. A second objective of this study is to subject the resulting algebraic stress model to a wider testing as was done by NR with their model, and to directly compare calculations obtained with the present and the NR-model. Accordingly, both models are applied to developing and fully developed flow in a square duct and to the fully developed flow in a partially roughened rectangular channel studied experimentally by Hinze (1973). Several variations to the model are also tested, such as an algebraic stress treatment of the primary shear stresses $\overline{u_1 u_2}$ and $\overline{u_1 u_3}$ and different wall corrections to the pressure–strain model, and, besides direct comparisons of calculated streamwise and secondary velocities and Reynolds stresses with experiments, a comparison of the secondary- and primary-velocity-gradient terms is also presented. It should be mentioned here that the present algebraic stress model was used for calculating several test cases for the Stanford Conference on Complex Turbulent Flows (see Kline, Cantwell & Lilley 1982).

3. Mathematical model

3.1. *Mean-flow equations*

The three-dimensional equations governing the distribution of the mean velocity components in straight ducts may be expressed as follows:

continuity equation

$$\frac{\partial U_1}{\partial x_1}+\frac{\partial U_2}{\partial x_2}+\frac{\partial U_3}{\partial x_3}=0; \tag{5}$$

streamwise (or longitudinal) momentum equation

$$U_1\frac{\partial U_1}{\partial x_1}+U_2\frac{\partial U_1}{\partial x_2}+U_3\frac{\partial U_1}{\partial x_3}=-\frac{1}{\rho}\frac{\mathrm{d}\overline{P}}{\mathrm{d}x_1}-\frac{\partial\overline{u_1 u_2}}{\partial x_2}-\frac{\partial\overline{u_1 u_3}}{\partial x_3}+\nu\left(\frac{\partial^2}{\partial x_2^2}+\frac{\partial^2}{\partial x_3^2}\right)U_1; \tag{6}$$

momentum equations governing the secondary velocities U_2 and U_3

$$U_1\frac{\partial U_2}{\partial x_1}+U_2\frac{\partial U_2}{\partial x_2}+U_3\frac{\partial U_2}{\partial x_3}=-\frac{1}{\rho}\frac{\partial P}{\partial x_2}-\frac{\partial\overline{u_2^2}}{\partial x_2}-\frac{\partial\overline{u_2 u_3}}{\partial x_3}+\nu\left(\frac{\partial^2}{\partial x_2^2}+\frac{\partial^2}{\partial x_3^2}\right)U_2, \tag{7}$$

$$U_1\frac{\partial U_3}{\partial x_1}+U_2\frac{\partial U_3}{\partial x_2}+U_3\frac{\partial U_3}{\partial x_3}=-\frac{1}{\rho}\frac{\partial P}{\partial x_3}-\frac{\partial\overline{u_2 u_3}}{\partial x_2}-\frac{\partial\overline{u_3^2}}{\partial x_3}+\nu\left(\frac{\partial^2}{\partial x_2^2}+\frac{\partial^2}{\partial x_3^2}\right)U_3. \tag{8}$$

The symbols are defined in figure 4. The streamwise turbulent fluxes of momentum have been neglected, and the pressure gradient $\partial P/\partial x_1$ originally appearing in (6) has been replaced by the cross-sectional average pressure gradient $\mathrm{d}\overline{P}/\mathrm{d}x_1$. These boundary-layer approximations make the equations parabolic in the streamwise direction; physically this means that downstream events cannot influence the flow upstream. The parabolic equations are amenable to numerical forward-marching solution procedures which are particularly economic. The viscous terms are formally retained in the calculation, but they are of no importance because the equations are not integrated in the viscous sublayer. Rather this is bridged by empirical wall functions which will be introduced below.

In §3.2 a turbulence model is introduced for determining the Reynolds stresses $\overline{u_2^2}$, $\overline{u_3^2}$, $\overline{u_1 u_2}$, $\overline{u_1 u_3}$ and $\overline{u_2 u_3}$ appearing in the momentum equations. Special attention is given to the modelling of the stresses $\overline{u_2^2}$, $\overline{u_3^2}$ and $\overline{u_2 u_3}$ appearing in the equations governing the secondary motion.

3.2. *Turbulence model*

The derivation of the turbulence model starts from the modelled transport equation for the Reynolds-stress component $\overline{u_i u_j}$ given by Launder *et al.* (1975). When convection and diffusion of the Reynolds stresses are neglected (assumption of local equilibrium), this equation for $\overline{u_i u_j}$ reduces to

$$0 = \underbrace{-\overline{u_i u_l}\frac{\partial U_j}{\partial x_l} - \overline{u_j u_l}\frac{\partial U_i}{\partial x_l}}_{P_{ij}\,=\,\text{production}} \quad \underbrace{-\tfrac{2}{3}\delta_{ij}\epsilon}_{\text{dissipation}}$$

$$\underbrace{-c_1\frac{\epsilon}{k}(\overline{u_i u_j}-\tfrac{2}{3}\delta_{ij}k) - \alpha(P_{ij}-\tfrac{2}{3}\delta_{ij}P) - \beta(D_{ij}-\tfrac{2}{3}\delta_{ij}P) - \gamma\left(\frac{\partial U_i}{\partial x_j}+\frac{\partial U_j}{\partial x_i}\right)k}_{\text{pressure–strain or redistribution}}, \tag{9}$$

where

$$P \equiv -\overline{u_i u_k}\frac{\partial U_i}{\partial x_k}, \quad D_{ij} \equiv -\overline{u_i u_l}\frac{\partial U_l}{\partial x_j} - \overline{u_j u_l}\frac{\partial U_l}{\partial x_i}. \tag{10}$$

P is the production of turbulent kinetic energy $k = \frac{1}{2}\overline{u_i u_i}$. According to (9), the production of $\overline{u_i u_j}$ by the interaction of stresses and mean-velocity gradients is balanced by viscous dissipation as well as by an interaction between fluctuating pressure and fluctuating strain rate (pressure–strain term) which tends to make turbulence more isotropic. Some calculations were carried out with a model in which convection and diffusion of $\overline{u_i u_j}$ were not neglected altogether but related to convection and diffusion of the turbulent kinetic energy k according to a proposal by Rodi (1976) (zero on the left-hand side of (9) was replaced by $\overline{u_i u_j}/k(P-\epsilon)$). The results obtained with this model were not significantly different from those of the present model, which assumes local equilibrium.

The expression for the pressure–strain term is model 1 of Launder *et al.* The surface-proximity effect on the turbulent stresses is accounted for in this model by making the empirical constants functions of a dimensionless distance from the wall:

$$\alpha = 0.7636-0.06f, \quad \gamma = 0.182, \quad \beta = 0.1091+0.06f, \quad c_1 = 1.5-0.50f, \tag{11}$$

where f is a function of the dimensionless wall distance to be introduced shortly, which has a value of unity in the near-wall region and of zero remote from walls. The values of the constants have been chosen such that, when $f = 0$, the model yields the correct Reynolds-stress components for the nearly homogeneous shear flow of Champagne, Harris & Corrsin (1970), and, when $f = 1$, the relative magnitude of the stress components agrees with a consensus of near-wall data. Hence the model predicts the correct separation between $\overline{u_3^2}-\overline{u_2^2}$, which, as was discussed above, is the driving term for the secondary motion. Here is one of the main differences from the Launder–Ying (LY) model, which used a different model approximation for the pressure–strain term not accounting for wall-proximity effects and yielding a far too small separation between the components $\overline{u_3^2}$ and $\overline{u_2^2}$ near walls.

Constants different from those in (11) can be chosen, which are also in agreement with the Champagne *et al.* free-shear-layer and the near-wall consensus data within experimental uncertainty, but the use of these constants in the secondary-flow calculations produced only slightly different results. Hence, the original constants proposed by Launder *et al.* as given in (11) were retained.

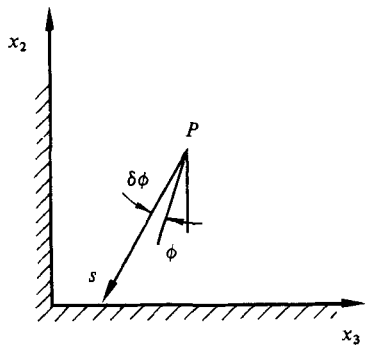

FIGURE 5. Notation for calculating average distance of point P from surface.

Launder *et al.* suggested the following linear relationship for the wall-damping function f:

$$f = \frac{L}{\langle y \rangle}, \quad \text{with} \quad \frac{1}{\langle y \rangle} = \frac{1}{2}\int_0^{2\pi} \frac{\mathrm{d}\phi}{s}, \tag{12}$$

where L is the lengthscale of the turbulent motion at the point considered and $\langle y \rangle$ is the average distance of this point from the surrounding surfaces as determined by the integral in (12) (see also figure 5). Naot & Rodi (1982) have shown that in the centre of a plane channel flow this damping function has a value of 0.8 of the value near the wall, suggesting strong wall influence even in the centre region. They argued that the wall-damping effect should decay faster with distance from the wall, and accordingly proposed the following quadratic relation:

$$f = \frac{L^2}{\langle y^2 \rangle}, \quad \text{with} \quad \frac{1}{\langle y^2 \rangle} = \frac{2}{\pi}\int_0^{2\pi} \frac{\mathrm{d}\phi}{s^2}. \tag{13}$$

According to this, the value of f at the centre of a plane channel is 0.3 times the value near the wall. Although the faster decay of the wall-damping function with distance from the wall appears more reasonable, it was not clear what the influence of this function on the actual calculation would be. Therefore calculations were carried out with both the linear and the quadratic wall-damping function, in order to examine the effect of the function. In both relations, the lengthscale L is determined from

$$L = \frac{c_\mu^3 k^3}{\kappa \epsilon}. \tag{14}$$

The coefficient c_μ^3/κ in this definition of L has been chosen so that f takes the value of unity in regions near plane walls where the logarithmic law of the wall prevails and the turbulence is in a state of local equilibrium (see §3.3 boundary conditions below).

Reece (1976) did not use the concept of an average distance for simulating the influence of a wall on the normal stresses. Rather, for rectangular channel flow, he assumed that the normal stress in the x_i direction is damped only by the wall normal to x_i, but is not influenced by the wall parallel to x_i. Accordingly, in calculating the function f to be used in (9) for the normal stresses in the cross-sectional plane, Reece used the distance from the wall normal to the stress considered. Some trial calculations using this approach have been carried out, but produced little difference to results obtained with the average distance as described above. In any case, it seems

reasonable that right in the corner the presence of the other wall should also have an influence on the fluctuations.

It is consistent with the local equilibrium assumption, already introduced into (9) to assume equality between production P and dissipation ϵ of turbulent kinetic energy, at least as far as the stress-relation (9) is concerned. Accordingly, P in (9) is replaced by ϵ to yield

$$(1-\alpha)\left(-\overline{u_i u_l}\frac{\partial U_j}{\partial x_l}-\overline{u_j u_l}\frac{\partial U_i}{\partial x_l}\right)+\beta\left(\overline{u_i u_l}\frac{\partial U_l}{\partial x_j}+\overline{u_j u_l}\frac{\partial U_l}{\partial x_i}\right)$$
$$-\gamma k\left(\frac{\partial U_i}{\partial x_j}+\frac{\partial U_j}{\partial x_i}\right)-\frac{\epsilon}{k}\left[c_1\overline{u_i u_j}+\tfrac{2}{3}(1-\alpha-\beta-c_1)\,\delta_{ij}k\right]=0. \quad (15)$$

When (15) is solved for the stress component appearing in the last bracketed term, there follows for the individual components

$$\overline{u_1^2}=\frac{2k}{c_1\epsilon}\left[\frac{\epsilon}{3}(\alpha+\beta+c_1-1)-(1-\alpha)\left(\overline{u_1 u_3}\frac{\partial U_1}{\partial x_3}+\overline{u_1 u_2}\frac{\partial U_1}{\partial x_2}\right)\right], \quad (16)$$

$$\overline{u_2^2}=\frac{\frac{2k}{c_1\epsilon}\left[\frac{\epsilon}{3}(\alpha+\beta+c_1-1)+\beta\overline{u_1 u_2}\frac{\partial U_1}{\partial x_2}-\overline{u_2 u_3}\left\{(1-\alpha)\frac{\partial U_2}{\partial x_3}-\beta\frac{\partial U_3}{\partial x_2}\right\}-\gamma k\frac{\partial U_2}{\partial x_2}\right]}{1+\frac{2k}{c_1\epsilon}(1-\alpha-\beta)\frac{\partial U_2}{\partial x_2}}, \quad (17)$$

$$\overline{u_3^2}=\frac{\frac{2k}{c_1\epsilon}\left[\frac{\epsilon}{3}(\alpha+\beta+c_1-1)+\beta\overline{u_1 u_3}\frac{\partial U_1}{\partial x_3}-\overline{u_2 u_3}\left\{(1-\alpha)\frac{\partial U_3}{\partial x_2}-\beta\frac{\partial U_2}{\partial x_3}\right\}-\gamma k\frac{\partial U_3}{\partial x_3}\right]}{1+\frac{2k}{c_1\epsilon}(1-\alpha-\beta)\frac{\partial U_3}{\partial x_3}}, \quad (18)$$

$$\overline{u_2 u_3}=\frac{k}{c_1\epsilon}\left[\beta\left(\overline{u_1 u_3}\frac{\partial U_1}{\partial x_2}+\overline{u_1 u_2}\frac{\partial U_1}{\partial x_3}\right)-\{(1-\alpha)\overline{u_2^2}-\beta\overline{u_3^2}+\gamma k\}\frac{\partial U_3}{\partial x_2}\right.$$
$$\left.-\{(1-\alpha)\overline{u_3^2}-\beta\overline{u_2^2}+\gamma k\}\frac{\partial U_2}{\partial x_3}\right], \quad (19)$$

$$\overline{u_1 u_2}=\frac{k}{c_1\epsilon}\left[\beta\overline{u_1 u_3}\frac{\partial U_3}{\partial x_2}-\{(1-\alpha)\overline{u_2^2}-\beta\overline{u_1^2}+\gamma k\}\frac{\partial U_1}{\partial x_2}\right.$$
$$\left.-(1-\alpha)\left(\overline{u_2 u_3}\frac{\partial U_1}{\partial x_3}+\overline{u_1 u_3}\frac{\partial U_2}{\partial x_3}\right)\right]\Big/\left[1+\frac{k}{c_1\epsilon}(1-\alpha-\beta)\frac{\partial U_2}{\partial x_2}\right], \quad (20)$$

$$\overline{u_1 u_3}=\frac{k}{c_1\epsilon}\left[\beta\overline{u_1 u_2}\frac{\partial U_2}{\partial x_3}-\{(1-\alpha)\overline{u_3^2}-\beta\overline{u_1^2}+\gamma k\}\frac{\partial U_1}{\partial x_3}\right.$$
$$\left.-(1-\alpha)\left(\overline{u_2 u_3}\frac{\partial U_1}{\partial x_2}+\overline{u_1 u_2}\frac{\partial U_3}{\partial x_2}\right)\right]\Big/\left[1+\frac{k}{c_1\epsilon}(1-\alpha-\beta)\frac{\partial U_3}{\partial x_3}\right]. \quad (21)$$

In deriving (16)–(21) from (15), the only approximation made is the boundary-layer one, according to which the velocity gradients in the streamwise direction x_1 can be neglected in developing flow. In developed flow, these gradients are of course exactly zero. It is important to note that the gradients of the secondary velocities with respect to x_2 and x_3 have been retained in the algebraic stress relations (16)–(21); following Launder & Ying (LY), these gradients were neglected in most other models. Naot & Rodi (NR) approximated the secondary-velocity-gradient terms in the numerators

of (17)–(19) for $\overline{u_2^2}$, $\overline{u_3^2}$ and $\overline{u_2 u_3}$ by the following eddy-viscosity expressions and neglected the secondary-velocity gradients in the denominator terms, making these unity:

$$\frac{k}{c_1 \epsilon}\left[\overline{u_2 u_3}\left\{(1-\alpha)\frac{\partial U_2}{\partial x_3}-\beta\frac{\partial U_3}{\partial x_2}\right\}+\gamma k\frac{\partial U_2}{\partial x_2}\right] \approx \nu_t \frac{\partial U_2}{\partial x_2}, \tag{22}$$

$$\frac{k}{c_1 \epsilon}\left[\overline{u_2 u_3}\left\{(1-\alpha)\frac{\partial U_3}{\partial x_2}-\beta\frac{\partial U_2}{\partial x_3}\right\}+\gamma k\frac{\partial U_3}{\partial x_3}\right] \approx \nu_t \frac{\partial U_3}{\partial x_3}, \tag{23}$$

$$\frac{k}{c_1 \epsilon}\left[\{(1-\alpha)\overline{u_2^2}-\beta\overline{u_3^2}+\gamma k\}\frac{\partial U_3}{\partial x_2}+\{(1-\alpha)\overline{u_3^2}-\beta\overline{u_2^2}+\gamma k\}\frac{\partial U_2}{\partial x_3}\right] \approx \nu_t\left(\frac{\partial U_3}{\partial x_2}+\frac{\partial U_2}{\partial x_3}\right). \tag{24}$$

How the eddy viscosity is determined will be discussed shortly.

The individual Reynolds-stress components are multiply coupled to each other by (16)–(21) and require in general an iterative procedure for their solution (or an even more expensive matrix inversion) at each downstream step of the forward-marching solution to be discussed below. Since this would make the calculation of developing flow very costly, and because a refined turbulence model is not so essential for calculating the primary shear stresses $\overline{u_1 u_2}$ and $\overline{u_1 u_3}$, the approach of existing models (e.g. LY and NR) is adopted to determine these stresses with the aid of the isotropic eddy-viscosity hypothesis:

$$-\overline{u_1 u_2} = \nu_t \frac{\partial U_1}{\partial x_2}, \tag{25}$$

$$-\overline{u_1 u_3} = \nu_t \frac{\partial U_1}{\partial x_3}, \tag{26}$$

where the streamwise velocity gradients have again been neglected. The differences between this method of determining the primary shear stresses and a method using the algebraic expressions (20) and (21) will be examined for developed channel flow, for which case results could be obtained with both methods. The isotropic eddy viscosity in (25) and (26) is calculated as in the conventional k-ϵ model by relating it to the turbulent kinetic energy k and the dissipation rate ϵ:

$$\nu_t = c_\mu \frac{k^2}{\epsilon}, \tag{27}$$

with $c_\mu = 0.09$ as in the standard k-ϵ model (see Rodi 1980). The quantities k and ϵ, which also appear in the algebraic stress relations (16)–(21), are calculated as in the k-ϵ model from the transport equations for these quantities:

$$U_1\frac{\partial k}{\partial x_1}+U_2\frac{\partial k}{\partial x_2}+U_3\frac{\partial k}{\partial x_3} = \frac{\partial}{\partial x_2}\left(\frac{\nu_t}{\sigma_k}\frac{\partial k}{\partial x_2}\right)+\frac{\partial}{\partial x_3}\left(\frac{\nu_t}{\sigma_k}\frac{\partial k}{\partial x_3}\right)+P-\epsilon, \tag{28}$$

$$U_1\frac{\partial \epsilon}{\partial x_1}+U_2\frac{\partial \epsilon}{\partial x_2}+U_3\frac{\partial \epsilon}{\partial x_3} = \frac{\partial}{\partial x_2}\left(\frac{\nu_t}{\sigma_\epsilon}\frac{\partial \epsilon}{\partial x_2}\right)+\frac{\partial}{\partial x_3}\left(\frac{\nu_t}{\sigma_\epsilon}\frac{\partial \epsilon}{\partial x_3}\right)+c_{\epsilon 1}\frac{\epsilon}{k}P-c_{\epsilon 2}\frac{\epsilon^2}{k}, \tag{29}$$

where

$$P = \nu_t\left[\left(\frac{\partial U_1}{\partial x_2}\right)^2+\left(\frac{\partial U_1}{\partial x_3}\right)^2+2\left(\frac{\partial U_2}{\partial x_2}\right)^2+2\left(\frac{\partial U_3}{\partial x_3}\right)^2+\left(\frac{\partial U_2}{\partial x_3}+\frac{\partial U_3}{\partial x_2}\right)^2\right] \tag{30}$$

is the production of k when the primary stresses are calculated from (25) and (26). When the primary stresses are determined from the algebraic stress relations (20) and (21), P is calculated from (10) with the stresses generated from (16)–(21) and only the terms with the streamwise velocity gradients neglected. $c_{\epsilon 1}$ and $c_{\epsilon 2}$ are empirical

constants, which have been given the standard values 1.44 and 1.92 respectively (see Rodi 1980). For compatibility of the model with the logarithmic law of the wall and the local equilibrium conditions, it is necessary for σ_ϵ to satisfy the constraint

$$\sigma_\epsilon = \frac{\kappa^2}{c_\mu^{\frac{1}{2}}(c_{\epsilon 1} - c_{\epsilon 2})}, \tag{31}$$

where κ is the von Kármán constant, with a value of 0.42 adopted here. Following Noat & Rodi (1982), $\sigma_k = \sigma_\epsilon = 1.225$ has been chosen, which deviates slightly from the values used in the extended k-ϵ model ($\sigma_k = 1.0$, $\sigma_\epsilon = 1.3$), but yields better agreement with the experimental eddy-viscosity distribution in developed plane channel flow.

Since the three normal stresses sum up to twice the turbulent kinetic energy k, the primary stress $\overline{u_1^2}$ is not calculated from the algebraic expression (16) but from k, $\overline{u_2^2}$ and $\overline{u_3^2}$. Equations (5)–(8), (17)–(19) and (25)–(30) form a closed set which needs to be solved simultaneously to determine the mean-velocity and Reynolds-stress components. How this was done will be discussed briefly in §3.3.

3.3. *Solution procedure and boundary conditions*

All the differential equations introduced above are parabolic in the streamwise direction, so that the solution cannot be influenced by downstream events and an efficient forward-marching solution procedure can be employed. This covers the calculation domain only once without iteration, starting from given conditions at an initial duct cross-section and requiring only two-dimensional storage of the dependent variables at the grid-points located in one cross-section. In particular, a modified version of the three-dimensional parabolic finite-difference procedure of Patankar & Spalding (1972) was employed. At the entry plane of the duct, a uniform distribution of all variables was prescribed. There the secondary velocities were set to zero and k and ϵ were given such small values that the eddy viscosity ν_t was about 10 times the molecular viscosity ν. Starting from these initial conditions, the step-by-step integration was carried out until developed flow was attained, that is the profiles did not change any more in the streamwise direction. At each step, the momentum equations were solved first with a guessed pressure field (guessed pressure gradient for the streamwise momentum equation (6)), where the prevailing upstream values were taken as guesses. The pressure and velocity fields were then corrected to satisfy the continuity equation (5). Subsequently, the Reynolds stresses were determined from the algebraic expressions (17)–(19) and from the eddy-viscosity relations (25) and (26) (or from (20) and (21)) with known upstream values of ν_t (or the stresses appearing on the right-hand side of the equations). As a last step, the k- and ϵ-equations (28) and (29) were solved. The error introduced by using upstream values of the turbulence quantities was found to be negligible when the forward step was less than 2.5% of the channel hydraulic diameter, in which case iteration at each step was unnecessary. The solutions were obtained with a 20×20 grid distributed non-uniformly over the cross-sectional plane. Test calculations were also carried out with a 30×30 grid, which, for developed square-duct flow, yielded secondary velocities which differed by less than 5% from those obtained with the coarser grid usually employed.

Boundary conditions need to be prescribed at symmetry planes and at solid walls. At symmetry planes, the velocity component normal to the symmetry plane was equal to zero, while for all other quantities the gradients normal to this plane were taken as zero.

At solid walls, the velocity normal to the wall was set equal to zero at the wall; otherwise, the wall function approach outlined by Launder & Spalding (1974) was adopted, which in effect means that the boundary conditions are not specified right at the wall but at a point outside the viscous sublayer where the logarithmic law of the wall prevails and the turbulence can be assumed to be nearly in local equilibrium. For such a point with distance y from the wall, the streamwise velocity U_1 and the lateral velocity U_ℓ are related to the friction velocity U_τ (strictly, U_τ is the resultant friction velocity, but this is nearly identical with the friction velocity in the x_1 direction):

$$U_1 = U_\tau \frac{1}{\kappa} \ln (Ey^+), \tag{32}$$

$$U_\ell = U_\tau \frac{1}{\kappa} \ln (Ey^+) \sin\theta, \tag{33}$$

where $y^+ = U_\tau y/\nu$, and θ is the angle between the resultant wall shear stress and the x_1 direction. κ is the von Kármán constant (here 0.42) and E is a roughness parameter, which was given the value 9.0 for smooth walls. In one of the applications with partially rough walls, a different value is used as will be discussed below. Noat & Rodi (1982) employed a modified form of (33) in order to account for the fact that the near-wall gradients of the lateral velocity U_ℓ are considerably steeper than described by the logarithmic law (33). However, this modification did not produce noticeably different results and is therefore not used here. The boundary conditions for k and ϵ are also specified at the first grid point where the logarithmic law of the wall prevails. With this and the assumption of local equilibrium there follows for a wall normal to x_3

$$k = \left(\frac{F_P}{c_\mu}\right)^{\frac{1}{2}} U_\tau^2, \quad \epsilon = F_P \frac{U_\tau^3}{\kappa y}, \tag{34}$$

where

$$F_P = 1 + \left(\frac{\partial U_1}{\partial x_2}\right)^2 \Big/ \left(\frac{\partial U_1}{\partial x_3}\right)^2. \tag{35}$$

For a wall normal to x_2, x_3 and x_2 should be exchanged. F_P accounts for the fact that, in corner regions, the generation of turbulent energy P given by (10) is influenced by the presence of both walls, while U_τ and y relate only to the wall nearest to the point in question. Hence F_P ensures that the production of kinetic energy is equal to the dissipation in the near-corner region; this would not be satisfied by the usual boundary condition (34), which uses $F_P = 1$. At the diagonal, F_P takes a value of 2, and hence (34) implies that the ratio k/U_τ^2 increases towards the corner. Gessner (1982) reports on measurements by Eppich which show the opposite trend. This trend is in conflict with the notion of local equilibrium (the shear layers along both walls contribute to the production of k) and could only be explained by a fairly strong convective transport of k by the secondary motion from the centre region with lower k into the corner. Note that the usual boundary condition ($F_P = 1$) would imply that the production is equal to twice the dissipation at the corner.

4. Results and discussion

4.1. *Square-duct flow*

The development of the flow in a square duct was calculated for various Reynolds numbers, starting with uniform streamwise and zero secondary velocities at the inlet ($x_1 = 0$).

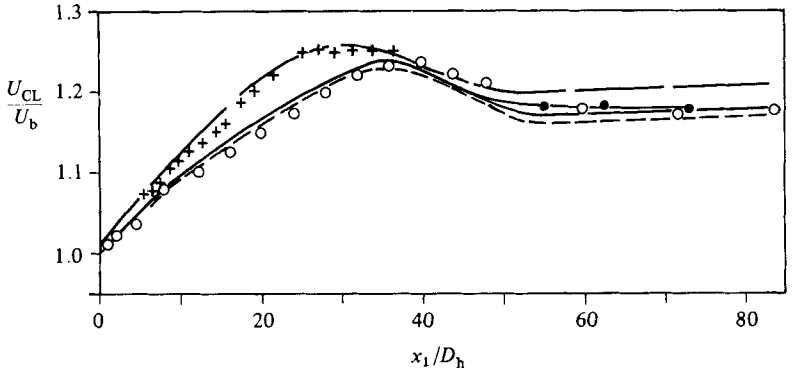

FIGURE 6. Flow development along axis of square duct. Data: +, Melling (1975), $Re = 42000$; ○, Gessner & Emery (1980), $Re = 250000$. Predictions: ——, present model, quadratic f-function, $Re = 50000$; —•—, present model, quadratic f-function, $Re = 250000$; ——, present model, linear f-function, $Re = 250000$; – – –, model of Naot & Rodi (1982).

Mean velocities

The calculated development of the streamwise velocity along the duct axis is shown in figure 6 for $Re = 50000$ *and* 250000, where it is compared with the measurements of Melling (1975) and Gessner & Emery (1980) taken at $Re = 42000$ and 250000 respectively. In agreement with the data, the velocity at the axis can be seen to rise first up to a maximum, and then to decrease and level off to an asymptotic value. The two calculations with the present model (linear and quadratic wall-damping functions) differ only slightly, while the NR-model produces somewhat lower velocities. On the whole, all three models predict satisfactorily the flow development. The fairly strong Reynolds-number influence, that is, the shift of the maximum from approximately $38D_h$ to $28D_h$, is also simulated well by the present model.

Figures 7 (*a*), (*b*) compare calculated and measured streamwise velocity distributions along the wall and corner bisector of a square duct at six downstream stations. There is no appreciable difference between the calculations performed with the linear and the quadratic wall-damping function, so that only one calculation is presented. Calculations obtained with the NR-model show significant differences from those with the present model only in the near-wall region. The predictions are compared mainly with the data of Po (1975) and Gessner (see Gessner & Emery 1980). The two sets of data were obtained in the same experimental apparatus and under similar conditions, so that the difference between them is a good measure of the experimental scatter. Along the wall bisector, the agreement between the predictions and the data is good in the developing region up to $24D_h$, particularly when the data of Gessner are taken for comparison. Further downstream, there is a tendency of the models to overpredict the velocity somewhat, particularly in the centre region. The fully developed profile (obtained for the smaller Reynolds number of 83000) is compared with the measurements of Brundett & Baines (1964) at $260D_h$. At this Reynolds number, the fully developed profile along the wall bisector can be seen to be in fairly good agreement with the data.

All the models also predict the velocity along the corner bisector fairly well down to $40D_h$. Further downstream, the present model tends to underpredict the velocity in the corner region, while the NR-model tends to overpredict it. Two contours of the primary velocity ($U_1/U_{1\max} = 0.8$ and 0.9) as predicted by the present model, the NR-model and the isotropic k-ϵ model at $x_1/D_h = 40$ and 84 are compared with

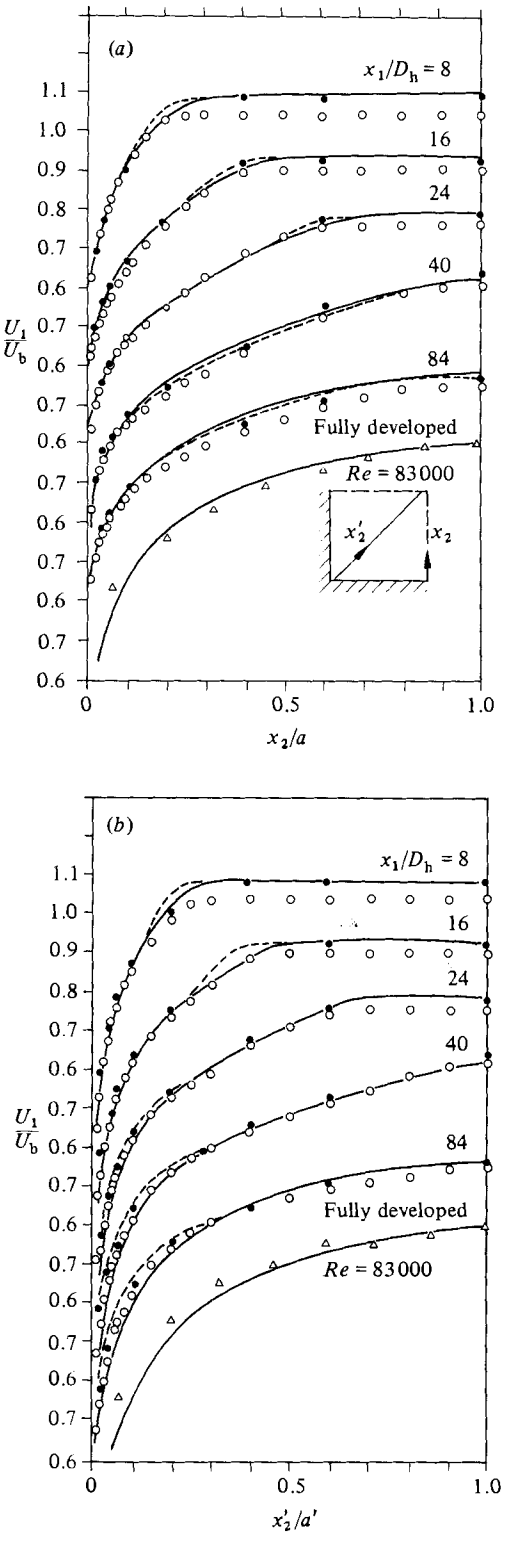

FIGURE 7 (*a*, *b*). For caption see p. 208.

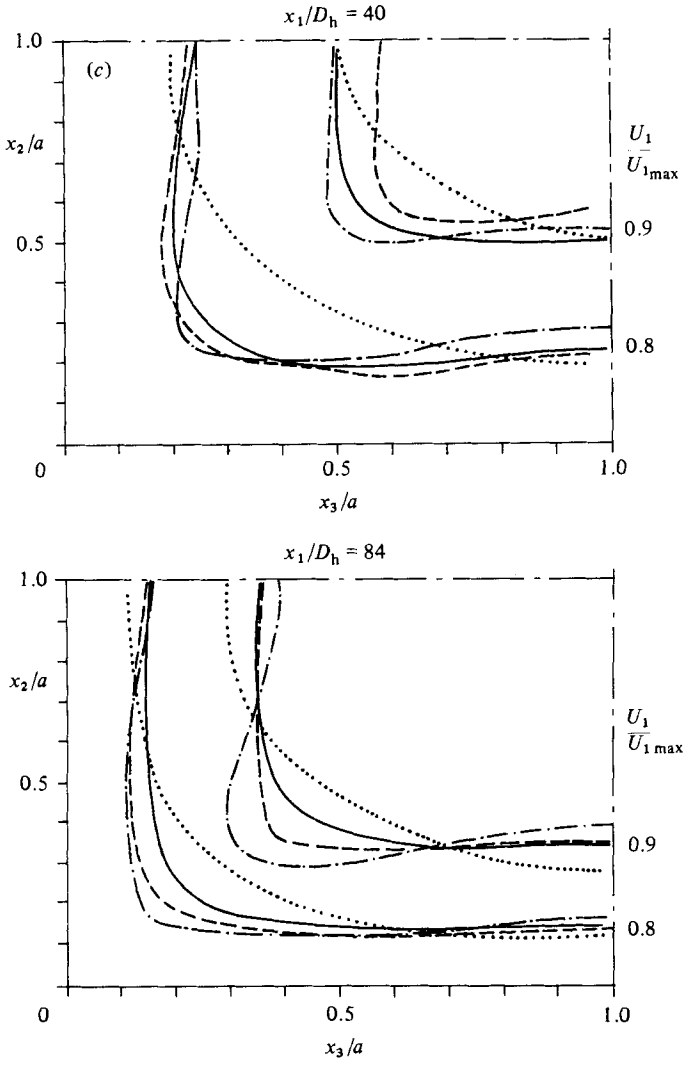

FIGURE 7 (*a*). Primary-velocity profiles along wall bisector, $Re = 250000$. Data: ○, Po (1975); ●, Gessner (in Gessner & Emery 1980); $Re = 83000$; △, Brundett & Baines (1964). Predictions: ——, present model; – – –, NR-model. (*b*) Primary-velocity profiles along corner bisector; symbols as in (*a*). (*c*) Primary-velocity contours of $U_1/U_{1max} = 0.8$ and 0.9. Data: —·—, Gessner (in Kline *et al.* 1982). Predictions: ——, present model; – – –, NR-model; ....., isotropic k-ϵ model. (Note that the scale is not the same in the x_2 and x_3 directions.)

the experimental data of Gessner and coworkers (see Kline *et al.* 1982) in figure 7 (*c*). At $x_1/D_h = 40$ predictions obtained with the present model agree quite well with the data, but at $x_1/D_h = 84$ they show too little bulging of the velocity contours towards the corners. At both locations the predictions obtained with the NR-model exhibit more bulging, and, in view of the uncertainties about the experimental contours discussed above (see figure 1) can be considered in fair agreement with the data. The reason for the differences lies in the predicted secondary motion as will be shown next. The isotropic k-ϵ model predicts no secondary motion at all, and thus the primary velocity contours are almost circular.

For $x_1/D_h = 40$ and 84 figure 8 compares predicted and measured secondary-velocity

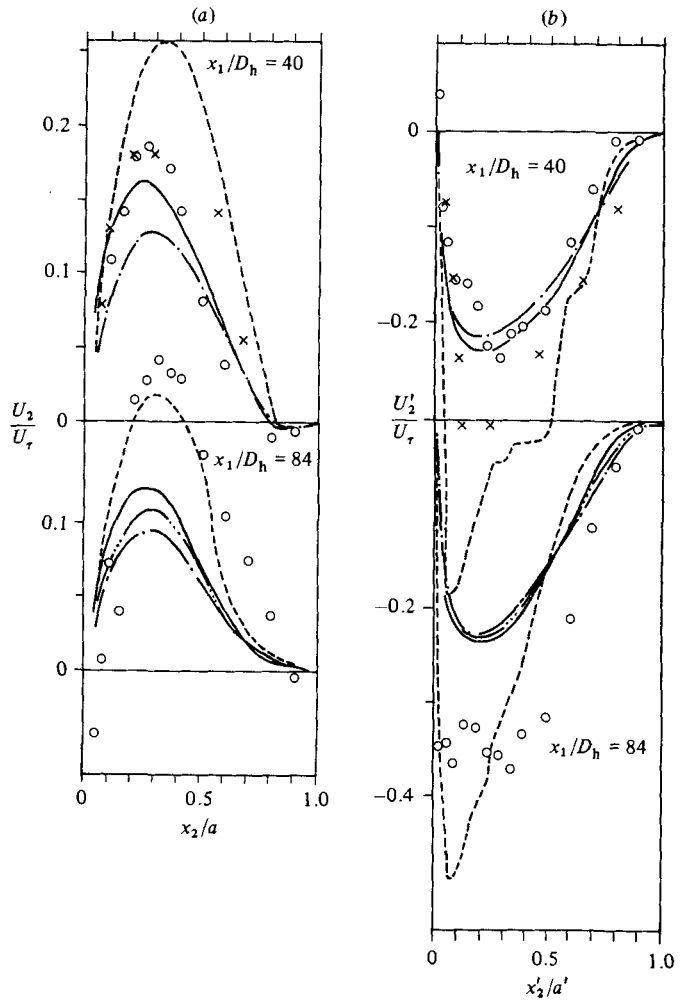

FIGURE 8. Secondary-velocity profiles. Data: ○ Gessner (in Gessner & Emery 1980); ×, Melling (1975). Predictions as in figure 6; —···—, present model with primary shear stresses from algebraic stress relations (20) and (21). (*a*) Wall bisector; (*b*) corner bisector.

distributions along the wall and corner bisectors. The data are due to Gessner, but at $x_1/D_h = 40$ the data of Melling (1975) have been included, even though they were taken at $x_1/D_h = 36.8$. There is fairly good agreement between the two data sets on the profile along the wall bisector, and here the measured maximum velocity of Gessner increases only slightly from $x_1/D_h = 40$ to 84. All the calculations show the opposite trend, that is U_2 decreases from $x_1/D_h = 40$ to 84. At both stations the present model underpredicts the secondary velocity, while the NR-model overpredicts the secondary velocity at $x_1/D_h = 40$ but produces about the right level of U_2 at 84. There is much less agreement between Gessner's and Melling's measured profiles along the corner bisector, which indicates a quite different flow development. Gessner's data at $x_1/D_h = 40$ are significantly lower than Melling's at $x_1/D_h = 36.8$; the flow takes 84 diameters to reach (and actually to exceed somewhat) the U_2 level observed much further upstream by Melling. The drastic increase in secondary velocity between $x_1/D_h = 40$ and 84 appears somewhat anomalous; it may have to do with the

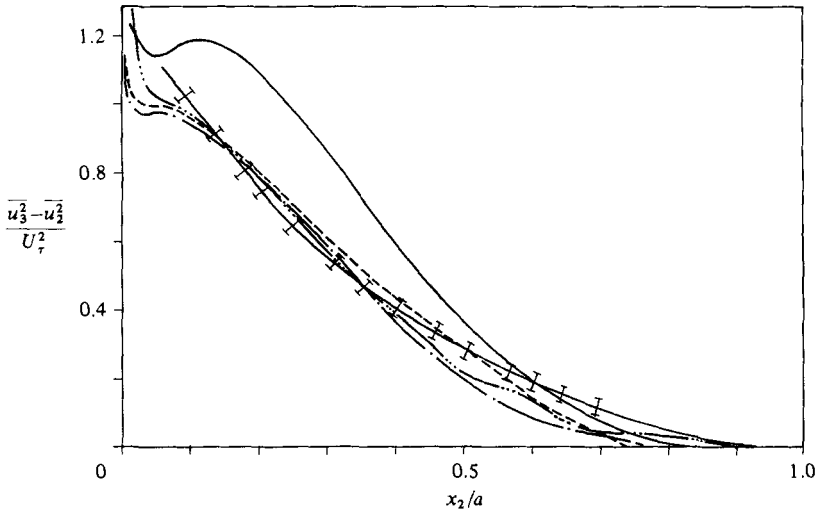

FIGURE 9. Separation of the secondary normal stresses, ⊣⊢, spread of corner-flow data (Perkins 1970). Predictions: see figures 6 and 8 for key to symbols.

formation of a counter-rotating secondary eddy near the bottom wall, which is indicated by the negative U_2 velocity in figure 8(*a*), but there is some uncertainty about this experimental finding. The present model predictions are in agreement with Gessner's data at $x_1/D_h = 40$, but they fall below Melling's data. At $x_1/D_h = 84$ they are also significantly below Gessner's data. On the other hand, the NR-model overpredicts the secondary velocity in the corner at both stations, by a rather large extent at the station $x_1/D_h = 40$.

The use of a linear instead of a quadratic wall-damping function increases the secondary velocities along the wall bisector by 20–30 %, but has little influence on the velocities along the corner bisector. Similarly, the calculation of the primary shear stresses $\overline{u_1 u_2}$ and $\overline{u_1 u_3}$ from the algebraic expressions (20) and (21) instead of the eddy-viscosity formula (25) and (26) leads to an increase in secondary velocity of about 10 % along the wall bisector but has no significant influence on the results along the corner bisector. It therefore appears that no serious error is made when the eddy-viscosity approximations are used for the primary shear stresses. As the secondary motion convects high-momentum fluid from the centre towards the corner and low-momentum fluid from the wall towards the centre, underprediction of the secondary velocity causes the streamwise velocity to be too low near the corner and too high near the centre, while overprediction of the secondary motion has the opposite effect. This explains why the present model produces slightly too high primary velocities near the centre and too low values in the corner region, while the NR-model predicts too high values in the corner. The developed secondary velocity profiles are included in figure 3, which also shows the underprediction by the present model and the overprediction by the NR-model, although these trends are less pronounced in the developed state.

The reasons for the different secondary motions predicted by the various models will now be examined. Figure 9 shows the predicted separation of the normal stresses, made dimensionless with the local friction velocity $(\overline{u_3^2}-\overline{u_2^2})/U_\tau^2$, along the wall bisector for the model variants used. The reader is reminded that it is this quantity for which the LY-model yields values that are too small by a factor of 10. A consensus

of near-wall data presented by Perkins (1970) is included in figure 9 for comparison. Except for the calculation using a linear near-wall damping function, all the models yield results that lie within the range of the experimental data for most of the channel. There is some deviation near the channel centre, where the assumption of local equilibrium made in the model is least valid. The linear damping function can be seen to lead to a separation of the normal stresses which is too large. This is due to the fact that the influence of the wall does not decay sufficiently fast with distance from the wall, as was pointed out already by NR. This finding lends support to the use of a quadratic wall-damping function instead of a linear one. The larger separation of normal stresses is responsible for the higher secondary motion predicted with the latter.

The present and the NR-model (both with quadratic f-function) predict similar separation of the normal stresses but considerably different secondary motion. The models differ in the treatment of the secondary-velocity gradients appearing in the algebraic stress expressions (17)–(19). In the NR-model the secondary-velocity-gradient terms are approximated by (22)–(24), while the denominators in (17) and (18) are replaced by unity. The calculations show that the denominator varies between 0.97 and 1.03 in the equations for $\overline{u_2^2}$ and $\overline{u_3^2}$. It is therefore mainly the approximations (22)–(24) that introduce the differences between the present and the NR-model. As will be shown later, the secondary-velocity-gradient terms in the $\overline{u_2 u_3}$ equation are the ones of prime importance. In the corresponding approximation (24), the left-hand side may be represented by a non-isotropic eddy-viscosity relation, while the right-hand side is an isotropic one. When the left-hand side is written in eddy-viscosity form, introducing the Prandtl–Kolmogorov formula (27), the c_μ coefficients of the two contributions are given by

$$c_{\mu 2} = \frac{1-\alpha}{c_1}\frac{\overline{u_2^2}}{k} - \frac{\beta}{c_1}\frac{\overline{u_3^2}}{k} + \frac{\gamma}{c_1}, \tag{36}$$

$$c_{\mu 3} = \frac{1-\alpha}{c_1}\frac{\overline{u_3^2}}{k} - \frac{\beta}{c_1}\frac{\overline{u_2^2}}{k} + \frac{\gamma}{c_1}. \tag{37}$$

Figure 10 shows the variation of $c_{\mu 2}$ calculated from the present model for fully developed flow. $c_{\mu 2}$ can be seen to range from 0.15 to 0.3, and this should be compared with the constant coefficient $c_\mu = 0.09$ used on the right-hand side of (24) in the NR-model. As the secondary-velocity-gradient term in the $\overline{u_2 u_3}$ expression acts to damp the secondary motion, the present model introducing effectively larger c_μ values leads to smaller secondary velocities. In the other extreme, when this term is neglected, the secondary motion is not sufficiently damped and keeps increasing during the solution process so that no stable solution can be reached, except when the production terms are significantly reduced.

The relative magnitudes of the secondary to the primary velocity-gradient terms in the algebraic stress relations (17)–(19) for $\overline{u_3^2} - \overline{u_2^2}$ and $\overline{u_2 u_3}$ are compared for the present model in figure 11. Considering the difference in the normal stresses, the magnitudes of the secondary-gradient terms are less than half those of the primary ones over most of the flow domain. However, in the shear-stress relation, the terms involving secondary gradients are larger than those involving primary ones over two-thirds of the flow domain, and the secondary-gradient terms are particularly important in the midregion near the wall. The neglect of the secondary-gradient terms in the $\overline{u_2 u_3}$ relation is therefore by no means justified, and, as experience has shown, must be compensated for by other measures. The calculations have shown that the

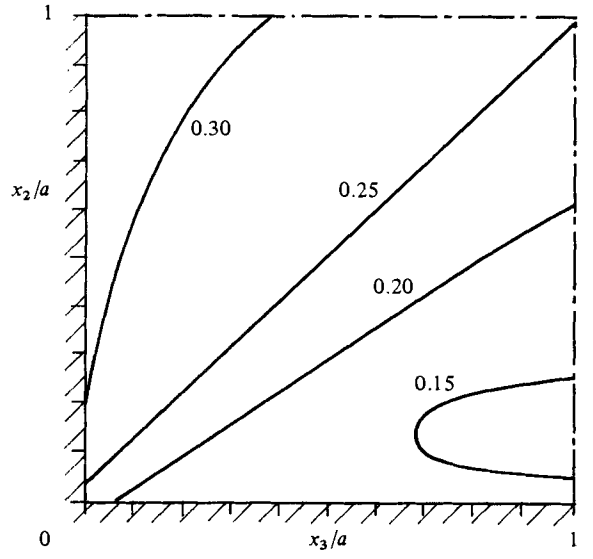

FIGURE 10. Contours of $c_{\mu 2}$ computed from (36).

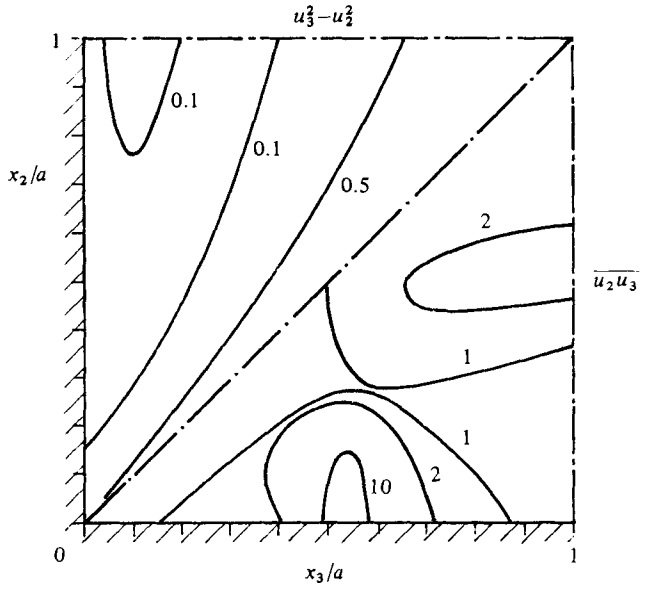

FIGURE 11. Contours of ratio of secondary to primary velocity-gradient terms in Reynolds-stress model (equations (17) and (18) for $\overline{u_2^2}$ and $\overline{u_3^2}$; (19) for $\overline{u_2u_3}$).

shear-stress term in the momentum equations for the secondary motion is generally of the same order as the normal-stress term, which is the reason for the predicted secondary motion to be very sensitive to the modelling of the shear-stress term. In order to give an impression of the relative magnitude of the terms in the momentum equations for the secondary motion, the variation of the individual terms in the U_3 equation along the first grid line ($x_2/a = 0.02$) is plotted in figure 12. It is clear from this figure that the shear-stress term is in most regions larger than the normal-stress terms. In the corner region, which is most important for the secondary-flow

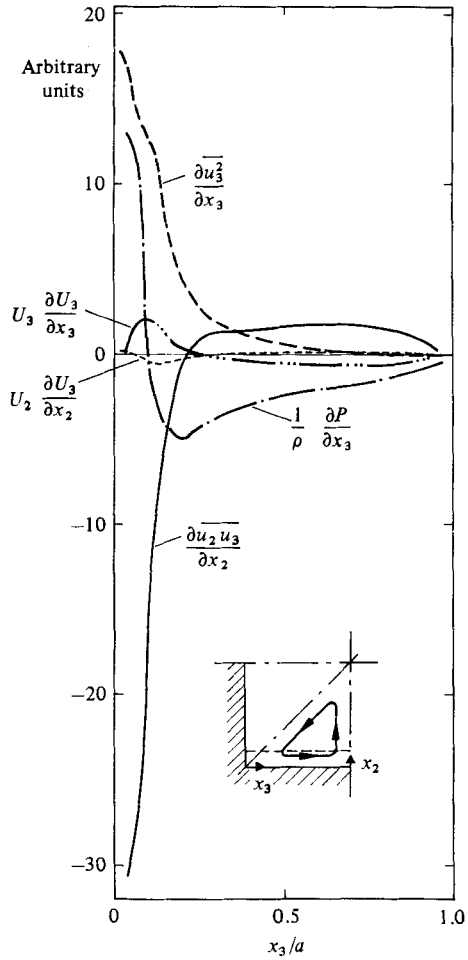

FIGURE 12. Balance of terms in x_3 momentum equation along first gridline ($x_2/a = 0.02$).

mechanism, the shear-stress and normal-stress terms are of comparable magnitude and of opposite sign, and the convection terms are one order of magnitude smaller. The viscous terms turned out to be so small that they would not show up on the graph. These observations support the conclusions drawn in §2 on the dominant terms in the secondary-flow equations. Of course, here a momentum equation is considered which involves as one of the important terms the pressure gradient; hence a direct analogy with the vorticity equation (3) and the terms in it is not appropriate. However, the distribution of terms in figure 12 is qualitatively similar to that determined by Gessner & Jones (1965) for the terms in a momentum equation for the velocity component along a secondary-flow streamline. Too close a similarity should not be expected because figure 12 concerns the momentum equation for a velocity component with fixed direction.

Turbulence quantities

Figure 13 compares the predicted and measured development of the turbulent kinetic energy k along the wall and corner bisectors. In the central part of the channel, the agreement is fairly good, but there are certain discrepancies near the wall and

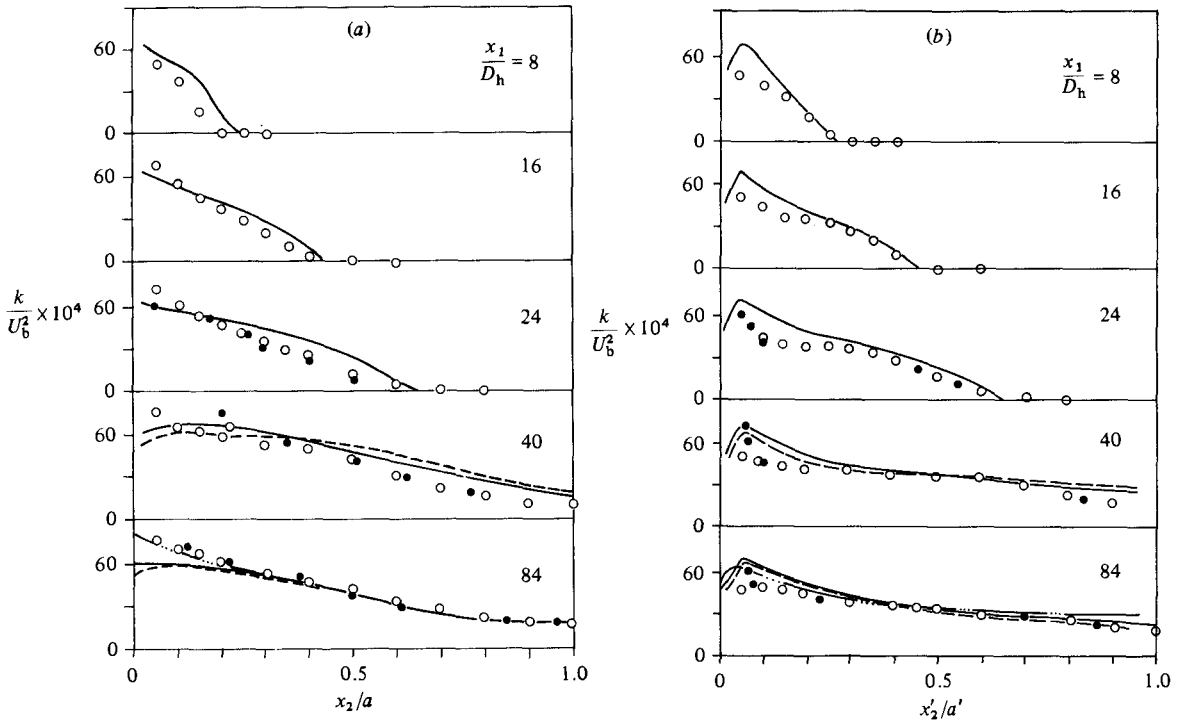

FIGURE 13. Turbulent-kinetic-energy profiles, $Re = 250000$. Data: ○, Po (1975); ●, Gessner (in Gessner & Emery 1980). Predictions: ——, present model; —···—, present model with primary shear stresses from algebraic stress relations (20) and (21); – – –, NR- model. (*a*) Wall bisector; (*b*) corner bisector.

in the corners. In figure 13(*a*) the present and the NR-model can be seen to yield low values of k near the wall. Both models use a value of $c_\mu = 0.09$ in the relation (34) that determines the k-value at the first grid point away from the wall. This standard value of c_μ is known to be too high as it takes no account of the damping of the normal fluctuations and the associated reduction in momentum transfer in the immediate vicinity of the wall (see Ljuboja & Rodi 1980). Figure 13(*a*) also shows that the model version that calculates the primary shear stresses directly from the algebraic expressions (20) and (21) yields the correct k near the wall. Through the wall-damping function in these expressions, c_μ is reduced in the vicinity of the wall; this reduced value of c_μ is also used in the boundary condition (34) and leads to a higher k-value at the first grid point.

In the corner, the predicted k-values are higher than the measured ones, except at the first grid point. At this point, the velocity gradient appearing in the production of k is forced to be roughly in agreement with experimental findings as it follows from the log law (32) applied to this point. At the next grid point away from the wall, however, the velocity gradient is determined as part of the solution, and since this gradient is overpredicted to some extent (see figure 7*b*) too much kinetic energy is produced, which leads to the higher predicted peak values of k. Furthermore, the measurements reported by Gessner (1982) indicate that the ratio of k to U_τ^2 decreases as the corner is approached while the local-equilibrium arguments leading to the condition (34) imply an increase of this ratio.

Figure 14 compares the predicted and measured shear stress $\overline{u_1 u_2}$ along the wall

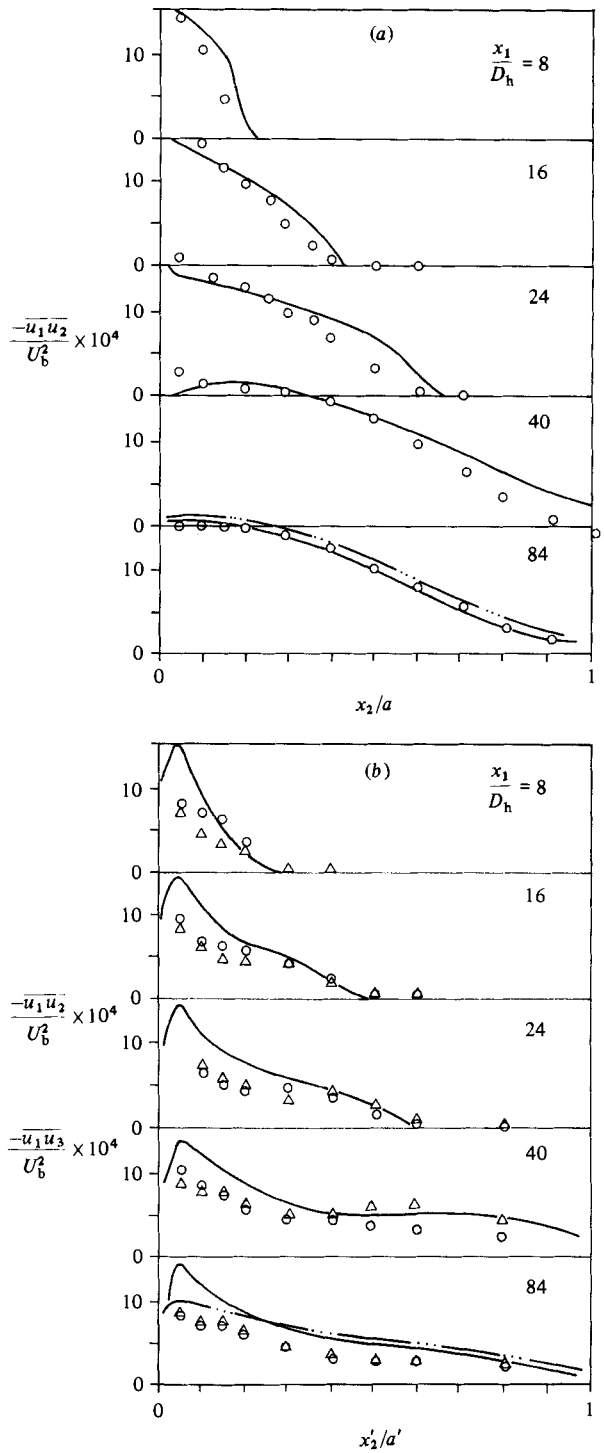

FIGURE 14. Primary-shear-stress profiles. (*a*) Wall bisector: for key to symbols see figure 13. (*b*) Corner bisector; ○, $-\overline{u_1 u_2}$; △, $-\overline{u_1 u_3}$.

and corner bisectors. Along the latter, this shear stress is equal to the shear stress $\overline{u_1 u_3}$, for which the measurements are also included in figure 14(*b*). There is fairly good agreement along the wall bisector, but the distributions along the corner bisector (figure 14*b*) show some discrepancies. The values at the first grid points appear to be supported by the experiments but the peak at the second grid point away from the wall is not. This is likely to be caused again by too high velocity gradients at this point as discussed before in connection with the k-profile. The use of an algebraic shear-stress relation instead of the eddy-viscosity expression can be seen to reduce this peak significantly. The reason is that the normal fluctuations $\overline{u_2^2}$ appearing in the main production term in the $\overline{u_1 u_2}$ equation are reduced significantly by the wall-damping function present in the algebraic relations. It therefore appears that the use of the algebraic relations (20) and (21) for the primary shear stresses has a beneficial effect in the corner region. However, it should be mentioned again that these relations could only be employed for the fully developed flow calculations without excessive computational cost. Further, the overall effect of using this more refined model on the mean-flow calculations has been shown to be only slight.

Additional results of the square-duct calculations are presented in the proceedings of the Stanford Conference on Complex Turbulent Flows (Kline *et al.* 1982).

4.2. *Flow in partially rough rectangular channel*

As a second test, calculations were carried out for the fully developed turbulent flow in a 5:1 ratio rectangular channel studied experimentally by Hinze (1973). The lower of the long walls was roughened with elements having an average height of 0.004 m, but the central 22 % of this wall was left smooth. The channel geometry is illustrated in figure 15. The Reynolds number based on the maximum velocity was 1.5×10^5 in Hinze's experiment. The measurements were carried out only at a cross-section 126 hydraulic diameters from the inlet, and most quantities were measured only along the wall bisector ($x_3 = 0$). The change in roughness of the lower wall was found to produce considerably higher secondary motion than in channels with smooth walls, as can be seen in figure 15 from the fairly strong distortion of the velocity contours over the smooth part of the lower wall. Near the rough wall, higher turbulent stresses are generated in contrast to the region over the smooth part of the lower wall so that fairly strong gradients of stresses exist, including those of $\overline{u_2^2}$, $\overline{u_3^2}$ and $\overline{u_2 u_3}$. These gradients, according to the longitudinal vorticity equation (3), induce the fairly high secondary velocities. These velocities transport turbulent kinetic energy from the region of high generation above the rough-wall section to the region with low generation above the smooth centre part, but this is a consequence of the secondary motion and not the cause of this motion as implied by Hinze (1973).

In the calculations, the roughness entered through the log law (32) relating the velocity at the first grid point away from the wall with the friction velocity. For the rough wall in Hinze's experiments, the logarithmic velocity law reads

$$U_1 = U_\tau \frac{1}{\kappa} \ln \frac{30y}{0.004}, \tag{38}$$

which corresponds to (32) when the roughness coefficient E has a value of 0.14. On all smooth-wall sections, the usual value of $E = 9.0$ was retained. The downstream integration of the equations was continued until developed flow had been reached, and the resulting streamwise velocity contours are compared with the measurements of Hinze in figure 15. On the left half of the figure, calculations obtained with the NR-model are compared with the data and on the right half the calculations obtained

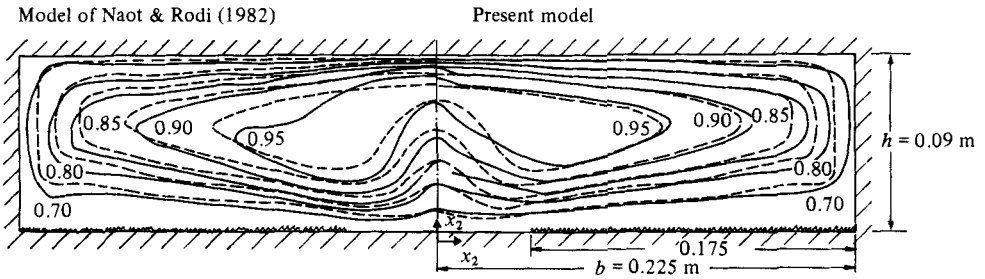

FIGURE 15. Contours of primary velocity $U_1/U_{1\max}$ in fully developed flow in partially rough rectangular channel. Data: ---, Hinze (1973). ——, Present predictions.

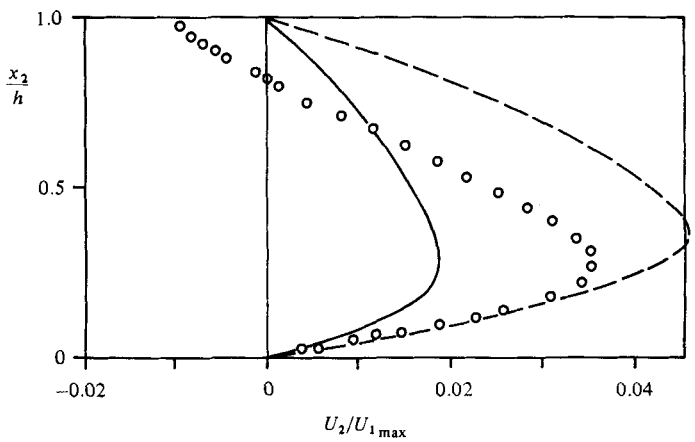

FIGURE 16. Secondary velocity along wall bisector in partially rough channel. Data: ○, Hinze (1973). Predictions: ——, present model; ---, NR-model.

with the present model. Both models can be seen to simulate the distortion of the velocity contours by the secondary motion quite well, and it is difficult to say which model yields the better agreement with the data. The present model underpredicts somewhat the displacement of the isovels in the vertical direction near the wall bisector, while the NR-model causes a somewhat too strong distortion. The reasons for these discrepancies can be found in the secondary motions, which are predicted too small by the present model and too large by the NR-model, as can be seen from figure 16, where the calculated secondary velocity is compared with measurements along the wall bisector. The present model leads to secondary velocities that are about 50 % smaller than the measured ones, a trend that is consistent with the performance in the case of the square-duct flow. The NR-model predicts the correct secondary velocity near the lower wall, but then overpredicts this velocity in the upper two-thirds of the channel. Both models do not produce any negative (i.e. downward) velocity near the upper wall as observed in the experiments. Apparently, a second counter-rotating eddy existed in the experiments which could not be resolved with either of the models. However, there appears to be no reflection of this eddy and the downward secondary motion on the velocity contours near the upper wall.

Figure 17 compares the calculated and measured k-profiles on the wall bisector. The strongly asymmetric behaviour of the k-profile is simulated well by both the present and the NR-model, with the minimum located near the upper wall where the

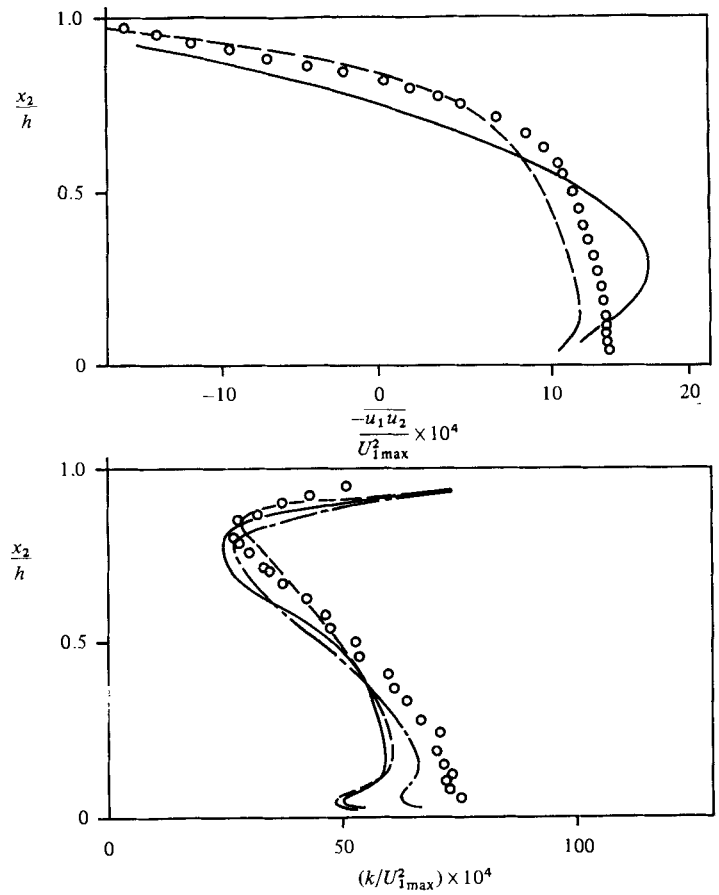

FIGURE 17. Turbulent shear stress and kinetic energy along wall bisector, for key to symbols see figure 16; —·—, present model with primary shear stress from algebraic stress relations (20) and (21).

mean velocity U_1 has a maximum. Agreement between measurements and predictions with both models is reasonable in the centre portion near the upper wall, but near the lower wall the calculated k-values fall considerably below the measured ones. Here the assumption of local equilibrium introduced to determine the k-value at the first grid point via relation (34) is certainly not valid because the fairly strong secondary motion convects k from the region above the rough walls to the centre portion with smooth wall, and in addition there may also be considerable diffusion of k towards the centre. In this case, the condition (34) applied at the first grid point is too crude and a more refined treatment is necessary. Figure 17 includes calculations obtained by determining the primary shear stresses from the algebraic relations (20) and (21) instead of the eddy-viscosity relations, which leads effectively to a lower value of c_μ in (34), as explained in §4.1. Accordingly, somewhat higher k-values are obtained near the lower wall, but this model still ignores the transport from the region with high production.

Figure 17 also compares calculated and measured shear-stress profiles along the wall bisector. The profile obtained with the present model is shifted somewhat towards the lower wall, and overshoots the measured profile in the lower half of the

duct. This is due to the fact that the velocity contours are not distorted sufficiently so that the velocity maximum is too close to the lower wall and, associated with this, the velocity gradient is too large near the lower wall. As the NR-model predicts a significantly larger secondary motion and hence also a larger distortion of the velocity contours, the velocity maximum is roughly at the measured position, and the shear-stress distribution is in much better agreement with measurements. In both models, the shear stress very near the lower wall is smaller than the measured one, and this is a consequence of the kinetic energy k and hence also the eddy viscosity ν_t being underpredicted near the lower wall for reasons explained above. It should be added that Hinze also measured the distribution of the dissipation rate ϵ along the wall bisector and that the calculated ϵ-distribution agrees very well with these measurements.

5. Conclusions

The review of measurements on secondary flow in square ducts presented in this paper has shown that, in the equation for the streamwise vorticity, the terms involving the separation between the turbulent normal stresses $\overline{u_3^2}-\overline{u_2^2}$ and the shear stress $\overline{u_2 u_3}$ are of the same order of magnitude and of opposite sign. They are much larger than all the other terms in the equation, and it is the difference between these terms that is of the same order of magnitude as the convection term and is the mechanism that drives the secondary motion. Hence both terms must be modelled accurately in a calculation method in order to describe realistically the secondary flow. The algebraic stress model of Launder & Ying (1973), on which most other models are based, has been found to yield a separation between the normal stresses $\overline{u_3^2}-\overline{u_2^2}$ that is much smaller than that experimentally observed. The Launder–Ying model originates from the stress-equation model of Hanjalić & Launder (1972), which already underpredicts the normal-stress separation because it does not account for any wall-proximity effects on the turbulent fluctuations. By changing one of the empirical constants, this separation was further reduced in the Launder–Ying model in order not to overpredict the secondary motion. The paper has shown that this measure was necessary because, in their algebraic stress model, the secondary-velocity gradients were neglected. These gradients increase the $\overline{u_2 u_3}$ terms, thereby damping the secondary motion. These terms have been found to be very important in the algebraic expressions for $\overline{u_2 u_3}$ as they are larger than the terms due to the primary velocity gradients in over two-thirds of the flow domain.

An algebraic stress model has been introduced which is similar to the Launder–Ying model in that algebraic expressions for the Reynolds stresses $\overline{u_2^2}$, $\overline{u_3^2}$ and $\overline{u_2 u_3}$ were derived by simplifying modelled transport equations for the Reynolds stresses. However, the primary shear stresses $\overline{u_1 u_2}$ and $\overline{u_1 u_3}$ are determined from a standard eddy-viscosity relation. The differences are that the present model was derived from the stress-equation model of Launder *et al.* (1975), which involves a wall-proximity correction and leads to the correct separation between $\overline{u_3^2}$ and $\overline{u_2^2}$ with the original constants, and that the secondary-velocity-gradient terms were retained in the algebraic expressions. Two variants of this model have also been considered, one being due to Naot & Rodi (1982) in which the secondary-velocity-gradient terms were approximated by an eddy-viscosity relation, and the other using an algebraic stress model also for primary shear stresses $\overline{u_1 u_2}$ and $\overline{u_1 u_3}$ (although only for developed flow).

The application of the various model versions to developing square-duct flow has shown that all versions predict fairly well the development of the streamwise velocity

along the duct axis and its dependence on the Reynolds number. On the other hand, the present model overpredicts somewhat the streamwise velocity in the duct centre and underpredicts it in the corner region, while the Naot–Rodi (NR) model leads to velocities in the corner region that are somewhat high. These discrepancies are due to the fact that the present model underpredicts the secondary motion while the NR-model overpredicts it. The comparison with secondary-velocity measurements is somewhat inconclusive because significant differences between various measurements exist that await an explanation. The differences between the present model and the NR-model stem from the different treatment of the secondary-velocity-gradient terms in the $\overline{u_2 u_3}$ expression. The results are very sensitive to this treatment because of the large relative magnitude of these terms. The development of the turbulent kinetic energy k is simulated quite well in most regions, but near the wall the predicted k is somewhat too low, and near the corner it is too high. The predicted shear stress is also too high in the corner region, and the use of algebraic expressions for the primary shear stresses $\overline{u_1 u_2}$ and $\overline{u_1 u_3}$ improves the shear-stress predictions, but the overall effect on the calculations is slight. The model versions were also applied to the flow in a partially rough rectangular channel studied experimentally by Hinze (1973). In this case the secondary motion causes a strong distortion of the velocity contours, and this is simulated quite well by both the present model and the NR-model, the present one yielding a slightly too small distortion and the NR-model a slightly too large one. Again the respective underprediction and overprediction of the secondary motion by the two models is responsible for this.

The present model has been found to simulate many features of the flow in non-circular straight ducts satisfactorily, but it has a tendency to underpredict the secondary motion. The NR-model yields predictions of similar quality but shows the opposite trend, namely to somewhat overpredict the secondary motion. A pragmatic approach of improving the accuracy of the secondary-flow prediction for practical calculations would be to simply use a somewhat larger value for c_μ in the approximation of the secondary-velocity-gradient terms used in the NR-model. However, further work is necessary in order to develop a model for simulating accurately the secondary velocities without any tuning of constants.

The work reported here was sponsored by the Deutsche Forschungsgemeinschaft via the Sonderforschungsbereich 80. The calculations were carried out on the UNIVAC 1108 computer of the University of Karlsruhe, using a modified version of program FLAIR of CHAM Ltd, London, which is based on the algorithm of Patankar & Spalding (1972).

REFERENCES

ALY, A. A. M., TRUPP, A. C. & GERRARD, A. D. 1978 Measurements and prediction of fully developed turbulent flow in an equilateral triangular duct. *J. Fluid Mech.* **85**, 57–83.

ARNAL, D. & COUSTEIX, J. 1981 Turbulent flow in unbounded streamwise corners. In *Proc. 3rd Symp. on Turbulent Shear Flows, Davis, California.*

BRUNDETT, E. & BAINES, W. D. 1964 The production and diffusion of vorticity in duct flow. *J. Fluid Mech.* **19**, 375–394.

BULEEV, N. I. 1963 Theoretical model of the mechanism of turbulent exchange in fluid flows. *AERE Transl.* 957.

CHAMPAGNE, F. H., HARRIS, V. G. & CORRSIN, S. 1970 Experiments on nearly homogeneous turbulent shear flow. *J. Fluid Mech.* **41**, 81–139.

EINSTEIN, H. A. & LI, H. 1958 Secondary currents in straight channels. *Trans. Am. Geophys. Union* **39**, 1085–1088.

GESSNER, F. B. 1964 Turbulence and mean-flow characteristics of fully developed flow in rectangular channels. Ph.D. thesis, Dept. Mech. Engng, Purdue University.

GESSNER, F. B. 1973 The origin of secondary flow in turbulent flow along a corner. *J. Fluid Mech.* **58**, 1–25.

GESSNER, F. B. 1982 Corner flow (secondary flow of the second kind). In Kline *et al.* (1982), pp. 182–212.

GESSNER, F. B. & EMERY, A. F. 1980 The numerical prediction of developing turbulent flow in rectangular ducts. In *Turbulent Shear Flows 2* (ed. J. S. Bradbury, F. Durst, B. E. Launder, F. W. Schmidt, J. Whitelaw). Springer. [Also in *Trans. ASME* I: *J. Fluids Engng* **103** (1981), 445–455.]

GESSNER, F. B. & JONES, J. B. 1965 On some aspects of fully developed turbulent flow in a rectangular channel. *J. Fluid Mech.* **23**, 689–713.

GOSMAN, D. D. & RAPLEY, C. W. 1978 A prediction method for fully developed flow through non-circular passages. In *Numerical Methods in Laminar and Turbulent Flows* (ed. C. Taylor *et al.*). Pentech.

HANJALIĆ, K. & LAUNDER, B. E. 1972 A Reynolds stress model of turbulence and its application to thin shear flows. *J. Fluid Mech.* **52**, 609–638.

HINZE, J. O. 1973 Experimental investigation of secondary currents in the turbulent flow through a straight conduit. *Appl. Sci. Res.* **28**, 453–465.

HOAGLAND, L. C. 1960 Fully developed turbulent flow in straight rectangular ducts – secondary flow, its cause and effect on the primary flow. PhD thesis, Dept Mech. Engng, MIT.

KACKER, S. C. 1973 Discussion of 'prediction of flow and heat transfer in ducts of square cross-section'. *Proc. Inst. Mech. Engng* **187**, D147–D148.

KLEIN, A. 1981 Review: turbulent developing pipe flow. *Trans. ASME* I: *J. Fluids Engng* **103**, 243–249.

KLINE, S. J., CANTWELL, B. & LILLEY, G. M. (eds.) 1982 *Proc. 1980–81 AFORS – HTTM Stanford Conf. on Complex Turbulent Flows, Stanford University.*

LAUNDER, B. E., REECE, G. J. & RODI, W. 1975 Progress in the development of a Reynolds stress turbulence closure. *J. Fluid Mech.* **68**, 537–566.

LAUNDER, B. E. & SPALDING, D. B. 1974 The numerical computation of turbulent flow. *Comp. Meth. Appl. Mech. & Engng* **3**, 269–289.

LAUNDER, B. E. & YING. W. M. 1972 Secondary flows in ducts of square cross-section. *J. Fluid Mech.* **54**, 289–295.

LAUNDER, B. E. & YING, W. M. 1973 Prediction of flow and heat transfer in ducts of square cross-section. *Proc. Inst. Mech. Engrs* **187**, 455–461.

LJUBOJA, M. & RODI, W. 1980 Calculation of turbulent wall jets with an algebraic Reynolds stress model. *Trans. ASME* I: *J. Fluids Engng* **99**, 347–356.

LUND, E. G. 1977 Mean flow and turbulence characteristics in the near corner region of a square duct. M.S. thesis, Dept Mech. Engng, University of Washington.

MELLING, A. 1975 Investigation of flow in non-circular ducts and other configurations by laser Doppler anemometry. PhD thesis, University of London.

MELLING, A. & WHITELAW, J. H. 1976 Turbulent flow in a rectangular duct. *J. Fluid Mech.* **78**, 289–315.

NAOT, D. & RODI, W. 1982 Numerical simulations of secondary currents in channel flow. *J. Hydraul. Div. ASCE* **108** (HY8), 948–968.

NAOT, D., SHAVIT, H. & WOLFSHTEIN, M. 1974 Numerical calculation of Reynolds stresses in a square duct with secondary flow. *Wärme- und Stoffübertragung* **7**, 151–161.

NIKURADSE, J. 1930 Turbulente Strömung in nicht-kreisförmigen Rohren. *Ing. Arch.* **1**, 306–332.

PATANKAR, S. V. & SPALDING, D. B. 1972 A calculation procedure for heat, mass and momentum transfer in 3-D parabolic flows. *Intl J. Heat Mass Transfer* **15**, 1787–1806.

PERKINS, H. J. 1970 The formation of streamwise vorticity in turbulent flow. *J. Fluid Mech.* **44**, 721–740.

PRANDTL, L. 1926 Über die ausgebildete Turbulenz. *Verh. 2nd Int. Kong. für Tech. Mech., Zürich.* [Transl. *NACA Tech. Memo* 435, pp. 62–75.]

Po, J. K. 1975 Developing turbulent flow in the entrance region of a square duct. MS thesis, University of Washington.

Ramachandra, V. 1979 The numerical prediction of flow and heat transfer in rod-bundle geometries. PhD thesis, University of London.

Reece, G. J. 1976 A generalized Reynolds stress model of turbulence. PhD thesis, Imperial College, London.

Rodi, W. 1976 A new algebraic relation for calculating the Reynolds stresses. *Z. angew. Math. Mech.* **56**, T219–T221.

Rodi, W. 1980 *Turbulence Models and Their Application in Hydraulics.* Intl Assn for Hydraul. Res., Delft, The Netherlands.

Tatchell, D. G. 1975 Convection processes in confined three-dimensional boundary layers. PhD thesis, Imperial College, London.

Tracy, H. J. 1965 Turbulent flow in a three-dimensional channel. *J. Hydraul. Div. ASCE* **91**(HY6), 9–35.